

Sequential Bayesian Experimental Design for Prediction in Physical Experiments Informed by Computer Models

Hao Zhu* Markus Hainy*

March 18, 2026

Abstract

In many scientific and engineering domains, physical experiments are often costly, non-replicable, or time-consuming. The Kennedy & O’Hagan (KOH) model framework has become a widely used approach for combining simulator runs with limited experimental observations. Under Bayesian implementation, the simulator output, model discrepancy, and observation noise are jointly modeled by coupled Gaussian processes, followed by coherent posterior inference and uncertainty quantification. This work presents a genuinely sequential Bayesian experimental design (BED) framework explicitly aimed at improving the predictive performance of the KOH model. We employ a mutual information (MI)–based criterion and develop a hybrid variant that integrates with measures of local model complexity, leading to significantly more efficient design decisions. We further theoretically show that the MI-based criterion is more comprehensive and robust than the classical integrated mean squared prediction error (IMSPE) minimization criterion, especially when the model is highly uncertain in the early stages of the experiment. To mitigate the computational burden of the fully Bayesian inference and the ensuing BED process, we propose two acceleration strategies—Gaussian Mixture Compression and Schur complement & rank-one update—which together substantially reduce runtime. Finally, we demonstrate the effectiveness of the proposed methods through both a synthetic example and a real biochemical case study, and compare them against several classical design criteria under sequential (offline) and adaptive (online) BED settings.

Keywords: Bayesian experimental design; Kennedy and O’Hagan model; Mutual information; Sequential design; Gaussian process; local model complexity

1 Introduction

In many fields of science and engineering, computer models serve as simulators to enhance the understanding of real-world phenomena. They provide abstractions for the actual physical process and vary in level of accuracy. However, in many cases, computer models

*Institute of Applied Statistics, Johannes Kepler University Linz
Corresponding author email: hao.zhu@jku.at

inevitably deviate from the true physical process. Field data consequently play a crucial role in refining and calibrating computer models, as they correct model errors. However, acquiring field data, either from observations or through laboratory experiments, can be expensive and challenging. For instance, the discovery of new materials with a specific property often demands a significant number of costly and time-consuming experiments (Dehghannasiri et al., 2017). In these cases, gathering the most informative field data through optimal experimental design can significantly expedite the modeling process and lower the cost of the experiment.

Several well-established statistical frameworks have been developed to combine field data with simulation data (Cox et al., 2001; Higdon et al., 2004; Kennedy and O’Hagan, 2001). A common feature of these approaches is the use of a computationally cheaper emulator as a surrogate for the expensive mechanistic model. Our work builds on the Kennedy and O’Hagan (KOH) framework, which enables us to account for multiple sources of uncertainty, including model inadequacy and parameter uncertainty, within a Bayesian setting. Emulators are often constructed using nonparametric methods such as Gaussian processes (GPs) (Rasmussen and Williams, 2006) to capture the highly complex and nonlinear behavior of the physical system. Within this framework, computer models typically involve uncertain inputs which can be viewed as random variables that affect the overall simulation output. Such inputs are referred to as calibration parameters, while others are controllable by the experimenter. A natural way to improve the performance of computer models is through a more accurate calibration of their parameters.

Based on this idea, researchers have already proposed several optimal design methods in the KOH framework. Pratola et al. (2013) introduced an approach under expected improvement for sequential computer experiments, similar to the likelihood ratio, comparing the models with and without the discrepancy term. Huan and Marzouk (2013) utilized information-theoretic metrics to account for parameter uncertainty and formulated a Bayesian design for computationally intensive models as a continuous optimization problem. Arendt et al. (2015), using multivariate Gaussian sampling, developed a covariance-based preposterior approach for physical experiments. In Krishna et al. (2021), a hybrid strategy for physical experiments was built: a D-optimal design was used for parameter calibration and a space-filling design was used for model prediction under the Bayesian framework. More recently, Diao et al. (2022) suggested a sequential D-optimal design method for computer model calibration and compared its performance with other alternatives. Sürer et al. (2023) selected the expected integrated variance minimization of the calibration parameters as the criterion for sequential Bayesian design, considering the parameter uncertainty. A common difficulty is that the calibration parameters are typically multivariate and confounded with GP hyperparameters, which results in identifiability issues. To overcome this difficulty, Gu and Wang (2018), Wang et al. (2020), and Xie and Xu (2020) introduced projection-based methods that improve the identifiability of calibration parameters. Nevertheless, computer models still remain imperfect. In other words, even when all model parameters are accurately identified, systematic/structural model inadequacy relative to the true physical process often persists. For this reason, our work focuses not on parameter calibration, but on directly improving the KOH model’s overall predictive capability.

Indeed, several design criteria targeting objectives other than parameter calibration have also been proposed. However, little attention has been paid to methods that directly target

predictive performance. Among them, [Bayarri et al. \(2007\)](#) employed the Maximin Latin Hypercube Design (LHD) to conduct field experiments within a fully Bayesian framework. [Ranjan et al. \(2011\)](#) adopted the criterion of maximizing the reduction in the integrated mean squared error (IMSE) for physical experiments. [Williams et al. \(2011\)](#) compared several design criteria for simulator experiments, including maximum expected improvement and maximum entropy reduction. More recently, [Leatherman et al. \(2017\)](#) proposed a joint design strategy that combines the integrated mean squared prediction error (IMSPE) minimization with a nested maximin-augmented LHD to improve predictive accuracy. Building on this work, [Koermer et al. \(2024\)](#) derived a closed-form expression for IMSPE in the KOH model framework and reformulated it as a continuous gradient-based optimization problem for computer model design. Notably, these approaches are not information-theoretic and thus differ from fully Bayesian designs that aim to maximize expected information gain. When parameter and predictive uncertainties are fully accounted for, mutual information gain becomes the best tool to handle nonlinearity and potential multimodality ([Ryan et al., 2016](#)). Furthermore, explicit design methods for physical experiments across discrete inputs are largely absent from the literature. Most existing work instead targets computer model experiments, where the simulators are assumed to be operated over a continuous hypercube input space rather than a discrete set of feasible candidate points solving the design problem by using continuous optimization.

Bayesian experimental design (BED) was originally introduced by [Lindley \(1972\)](#) based on the decision-theoretic approach, and was later extended by [Chaloner and Verdinelli \(1995\)](#), who provided a comprehensive review and a coherent formulation framework applicable to various design objectives. [Higdon et al. \(2004\)](#) firstly developed a fully Bayesian estimation procedure for the KOH model, enabling an appropriate quantification of multiple sources of uncertainty. Most existing Bayesian design criteria are based on the Kullback–Leibler divergence between posterior and prior distributions, commonly referred to as the expected information gain (EIG). However, the computation of the EIG is notoriously challenging. To mitigate this problem, recent advances have introduced efficient gradient-based methods to optimize the variational lower bounds of the EIG ([Foster et al., 2019, 2020](#); [Kleinegesse and Gutmann, 2021](#)). Amortization strategies have also gained popularity in adaptive design ([Foster et al. \(2021\)](#)), where policy-based approaches in deep learning enable one-shot rather than step-by-step design studies. In line with Bayesian inference under the KOH framework, our objective is to conduct a BED with minimal simplifying assumptions so that all sources of uncertainty can be fully considered. This paper aims to fill this gap by proposing a genuinely sequential BED framework that explicitly focuses on designing physical experiments across discrete candidate locations. The proposed approach enhances the future predictive capability of the KOH model over successive design rounds and yields more efficient and robust designs than ad hoc approaches that neglect certain uncertainties.

This paper is organized as follows. Section 2 reviews the Kennedy & O’Hagan framework, summarizes its Bayesian implementation, and describes the design objectives in this work and some existing design criteria under the fully Bayesian approach. Section 3 introduces the mutual-information–based design criterion, along the extension we propose that incorporates local predictive complexity. Section 4 presents a set of strategies that substantially reduce the computational cost of the design. Section 5 evaluates the performance of all criteria considered in this work through both a synthetic toy example and a real-world dataset.

Section 6 concludes with a discussion of the findings of this paper and potential directions for future research.

2 Background and Related Work

In this section, we first provide a brief review of the KOH framework and its Bayesian implementation. Then, we introduce the design objectives and give an overview of previously employed experimental design criteria under the Bayesian framework. Further details are presented in the following subsections.

2.1 Review of Kennedy & O’Hagan Model

We adopt the computer model calibration framework proposed by [Kennedy and O’Hagan \(2001\)](#), along with its subsequent adaptations for fully Bayesian inference by [Higdon et al. \(2004\)](#) and [Bayarri et al. \(2007\)](#). The Kennedy & O’Hagan Model, hereafter denoted KOH model, is formulated as

$$\begin{aligned}\mathbf{y}^p &= y^c(\mathbf{X}^p, \boldsymbol{\theta}) + \delta(\mathbf{X}^p) + \boldsymbol{\epsilon}, \\ \mathbf{y}^s &= y^c(\mathbf{X}^c, \mathbf{T}).\end{aligned}$$

Throughout this article, vectors and matrices are denoted in boldface. Assume that we observe n responses from the physical process and m responses from the simulator, and let $N = n + m$ be the total number of design points (field + simulator). The controllable design inputs are represented by $\mathbf{X} = (\mathbf{X}^{c\top}, \mathbf{X}^{p\top})^\top = (\mathbf{x}_1^\top, \dots, \mathbf{x}_N^\top)^\top \in \mathbb{R}^{N \times d}$, with each $\mathbf{x}_i = (x_{i1}, \dots, x_{id})^\top \in \mathbb{R}^d$ denoting a single input location. Here, \mathbf{X}^c and \mathbf{X}^p correspond to the inputs of the computer model and the physical experiments, respectively. Let $\boldsymbol{\theta} = (\theta_1, \dots, \theta_h)^\top \in \mathbb{R}^h$ be the vector of the true calibration parameters and $\mathbf{T} = (\mathbf{t}_1^\top, \dots, \mathbf{t}_m^\top)^\top \in \mathbb{R}^{m \times h}$ be the design setting of the calibration parameters at which the simulator is evaluated. The underlying computer model is denoted by $y^c(\cdot, \cdot)$, and $\mathbf{y}^s \in \mathbb{R}^m$ represents the simulator outputs evaluated at a set of design points \mathbf{X}^c . Observations from the physical process are denoted by $\mathbf{y}^p \in \mathbb{R}^n$, with $\delta(\cdot)$ capturing the discrepancy between the physical process and the computer model (for multi-output cases, \mathbf{y}^p and \mathbf{y}^s can be matrix-valued, with each column corresponding to one task). The observational errors are assumed to be independent and normally distributed as $\boldsymbol{\epsilon} \sim \mathcal{N}(\mathbf{0}, \sigma^2 \mathbf{I}_n)$, where $\boldsymbol{\epsilon} = (\epsilon_1, \dots, \epsilon_n)^\top \in \mathbb{R}^n$. Both $y^c(\cdot, \cdot)$ and $\delta(\cdot)$ are modeled using Gaussian processes (GPs) ([Rasmussen and Williams, 2006](#)) under a Bayesian framework. Specifically, the two stages can be formulated as

$$y^c(\mathbf{X}^c, \mathbf{T}) \sim \text{GP}\left(m_c(\mathbf{X}^c, \mathbf{T}), K_{\phi_1}((\mathbf{X}^c, \mathbf{T}), (\mathbf{X}^c, \mathbf{T}'))\right), \quad (1)$$

$$\delta(\mathbf{X}^p) \sim \text{GP}\left(m_\delta(\mathbf{X}^p; \boldsymbol{\theta}), K_{\phi_2}(\mathbf{X}^p, \mathbf{X}^p')\right), \quad (2)$$

where $m_c(\cdot, \cdot)$ and $m_\delta(\cdot; \cdot)$ denote the mean functions, and $K_{\phi_1}(\cdot, \cdot)$ and $K_{\phi_2}(\cdot, \cdot)$ are the corresponding covariance kernels parameterized by hyperparameters ϕ_1 and ϕ_2 . For simplicity, we assume a zero-mean function for the first-stage (computer model) GP, so $m_c(\mathbf{X}^c, \mathbf{T}) = \mathbf{0}$ here.

Due to the properties of Gaussian processes (GPs), any finite collection of outputs follows a multivariate normal (MVN) distribution. In the KOH model, the outputs from the computer model and the physical process can be jointly expressed by a block-structured covariance matrix. Specifically, for the observed simulator runs \mathbf{y}^s and the physical observations \mathbf{y}^p , we have

$$\begin{pmatrix} \mathbf{y}^p \\ \mathbf{y}^s \end{pmatrix} \mid \boldsymbol{\theta}, \phi_1, \phi_2, \sigma^2 \sim \mathcal{N}(\boldsymbol{\mu}, \boldsymbol{\Sigma}_{oo}), \quad (3)$$

where $\boldsymbol{\mu} = (m_\delta(\mathbf{X}^p; \boldsymbol{\theta}), \mathbf{0}_m)^\top \in \mathbb{R}^N$ represents the mean and the joint covariance matrix $\boldsymbol{\Sigma}_{oo} \in \mathbb{R}^{N \times N}$ is decomposed as

$$\boldsymbol{\Sigma}_{oo} = \underbrace{\begin{pmatrix} \mathbf{K}_{c,pp} & \mathbf{K}_{c,ps} \\ \mathbf{K}_{c,sp} & \mathbf{K}_{c,ss} \end{pmatrix}}_{\text{computer GP}} + \underbrace{\begin{pmatrix} \mathbf{K}_{\delta,pp} & 0 \\ 0 & 0 \end{pmatrix}}_{\text{discrepancy GP}} + \underbrace{\begin{pmatrix} \sigma^2 \mathbf{I}_n & 0 \\ 0 & 0 \end{pmatrix}}_{\text{observation noise}}.$$

Here,

$$\mathbf{K}_{c,pp} = K_{\phi_1}((\mathbf{X}^p, \boldsymbol{\theta}), (\mathbf{X}^p, \boldsymbol{\theta})) \in \mathbb{R}^{n \times n}, \quad \mathbf{K}_{c,ps} = K_{\phi_1}((\mathbf{X}^p, \boldsymbol{\theta}), (\mathbf{X}^c, \mathbf{T})) \in \mathbb{R}^{n \times m},$$

$$\mathbf{K}_{c,ss} = K_{\phi_1}((\mathbf{X}^c, \mathbf{T}), (\mathbf{X}^c, \mathbf{T})) \in \mathbb{R}^{m \times m}, \quad \mathbf{K}_{\delta,pp} = K_{\phi_2}(\mathbf{X}^p, \mathbf{X}^p) \in \mathbb{R}^{n \times n}.$$

For prediction at a new set of design points $\mathbf{X}^* \in \mathbb{R}^{n^* \times d}$, we consider the joint distribution of the future outputs \mathbf{y}^* and observed data $\mathbf{y} = (\mathbf{y}^{p\top}, \mathbf{y}^{s\top})^\top$:

$$\text{Cov} \left[\begin{pmatrix} \mathbf{y}^* \\ \mathbf{y} \end{pmatrix} \right] = \begin{pmatrix} \boldsymbol{\Sigma}_{**} & \boldsymbol{\Sigma}_{*o} \\ \boldsymbol{\Sigma}_{o*} & \boldsymbol{\Sigma}_{oo} \end{pmatrix} \in \mathbb{R}^{(n^*+N) \times (n^*+N)}, \quad (4)$$

where

$$\boldsymbol{\Sigma}_{**} = K_{\phi_1}((\mathbf{X}^*, \boldsymbol{\theta}), (\mathbf{X}^*, \boldsymbol{\theta})) + K_{\phi_2}(\mathbf{X}^*, \mathbf{X}^*) + \sigma^2 \mathbf{I}_{n^*} \in \mathbb{R}^{n^* \times n^*},$$

$$\boldsymbol{\Sigma}_{*o} = [K_{\phi_1}((\mathbf{X}^*, \boldsymbol{\theta}), (\mathbf{X}^p, \boldsymbol{\theta})) + K_{\phi_2}(\mathbf{X}^*, \mathbf{X}^p) \quad K_{\phi_1}((\mathbf{X}^*, \boldsymbol{\theta}), (\mathbf{X}^c, \mathbf{T}))] \in \mathbb{R}^{n^* \times N},$$

and $\boldsymbol{\Sigma}_{o*} = \boldsymbol{\Sigma}_{*o}^\top$.

Consequently, the predictive distribution of \mathbf{y}^* conditional on observed data $\mathbf{y} = (\mathbf{y}^{p\top}, \mathbf{y}^{s\top})^\top$ is

$$\mathbf{y}^* \mid \mathbf{y}, \boldsymbol{\theta}, \phi_1, \phi_2, \sigma^2 \sim \mathcal{N}(\boldsymbol{\mu}^*, \boldsymbol{\Sigma}^*), \quad (5)$$

with predictive mean $\boldsymbol{\mu}^* \in \mathbb{R}^{n^*}$ and covariance $\boldsymbol{\Sigma}^* \in \mathbb{R}^{n^* \times n^*}$

$$\boldsymbol{\mu}^* = m_\delta(\mathbf{X}^*; \boldsymbol{\theta}) + \boldsymbol{\Sigma}_{*o} \boldsymbol{\Sigma}_{oo}^{-1} (\mathbf{y} - \boldsymbol{\mu}), \quad \boldsymbol{\Sigma}^* = \boldsymbol{\Sigma}_{**} - \boldsymbol{\Sigma}_{*o} \boldsymbol{\Sigma}_{oo}^{-1} \boldsymbol{\Sigma}_{o*}. \quad (6)$$

2.2 Design Objectives and Strategies

Optimal experimental design typically relies on constructing an appropriate design criterion or objective function. Such a criterion should either directly or indirectly represent the expected gain that the experimenter aims to achieve. As discussed earlier, the objective of this study is to select a set of design points for physical experiments that can improve the

predictive performance of the KOH model accounting for all sources of uncertainty within a BED framework. Compared to computer experiments, physical experiments are typically constrained by a limited set of candidate points and a tight experimental budget, which makes the design problem inherently discrete rather than a continuous optimization problem.

When real-time experiments cannot be conducted so that the model posterior cannot be updated, batch-optimal design, which simultaneously selects all experimental points within the given budget before the experiments, in principle performs at least as well as the sequential greedy approach and often yields better performance (Müller and Pötscher, 1992). However, as the number of candidate points increases, the combinatorial search space grows super exponentially, making true batch design computationally infeasible even for moderate problem sizes. The sequential greedy approach thus serves as a tractable approximation to the batch-optimal design, providing a practically efficient and theoretically interpretable alternative. Nemhauser et al. (1978) has established and theoretically proven a classical result for maximizing a non-negative, monotone submodular set function under a cardinality constraint. Under these conditions, the greedy algorithm can at least achieve a $(1 - 1/e \approx 63\%)$ approximation to the global optimal value. Building on this theorem, Krause et al. (2008) developed a greedy algorithm for sensor placement using a mutual-information criterion under a Gaussian process (GP) model, which empirically demonstrates that the greedy strategy can attain near-optimal performance. Their setting is closely related to ours, although our fully Bayesian GP framework is more complex and may not strictly satisfy the submodularity or monotonicity conditions. However, the greedy strategy remains a practically effective choice in our setting, as approximate monotonicity and submodularity are often sufficient for achieving high-quality results. In this study, we consider two strategies for multi-round Bayesian sequential experimental design: sequential (offline) design of experiments (SDE) and adaptive (online) design of experiments (ADE). The SDE is actually a greedy approach, seeking the best location at each round without incorporating information from future rounds.

Suppose we have a total budget of B physical experimental runs. Let $\mathcal{D}_{\text{cand}} = \{\boldsymbol{\xi}_1, \dots, \boldsymbol{\xi}_M\}$ denote the finite set of M candidate locations for conducting physical experiments, where each $\boldsymbol{\xi}_i \in \mathbb{R}^d$ represents a feasible experimental setting in the same input space as \mathbf{X}^p . Before iteration b , the subset of points already selected for experimentation is $\mathcal{D}_{\text{sel}}^{(b-1)} = \{\boldsymbol{\xi}_{(1)}, \dots, \boldsymbol{\xi}_{(b-1)}\}$, and the newly selected point in this round is $\boldsymbol{\xi}_{(b)} \in \mathcal{D}_{\text{cand}} \setminus \mathcal{D}_{\text{sel}}^{(b-1)}$. After completing all B rounds, the final design set is $\mathcal{D}_{\text{sel}}^{(B)} = \{\boldsymbol{\xi}_{(1)}, \dots, \boldsymbol{\xi}_{(B)}\}$. The predictive performance of the model is evaluated based on the predictive results \mathbf{y}^* at locations $\mathcal{X}_{\text{pred}} = \mathbf{X}^* \in \mathbb{R}^{n^* \times d}$.

Both the sequential design of experiments (SDE) and the adaptive design of experiments (ADE) proceed sequentially, selecting one new design input at a time according to a specified design criterion. In SDE, the optimal design input is determined sequentially based on the current KOH model, without performing any physical experiment. Consequently, the model posterior remains unchanged throughout the design process. In contrast, ADE conducts real physical experiments immediately after each selected design input. The corresponding observations then update the posterior before the next design input is chosen. Table 1 clearly illustrates the distinction between the two strategies.

Algorithm 1 Sequential (SDE) and Adaptive (ADE) Design under the KOH Framework

Require: Budget B ; candidates $\mathcal{D}_{\text{cand}} = \{\boldsymbol{\xi}_1, \dots, \boldsymbol{\xi}_M\}$; prediction set $\mathcal{X}_{\text{pred}} = \mathbf{X}^*$; initial data $\{(\mathbf{X}^p, \mathbf{X}^c, \mathbf{y})\}$; mode $\in \{\text{SDE}, \text{ADE}\}$; criterion or objective function $\text{Crit}(\cdot)$

Ensure: $\mathcal{D}_{\text{sel}}^{(B)} = \{\boldsymbol{\xi}_{(1)}, \dots, \boldsymbol{\xi}_{(B)}\}$

$\mathcal{D}_{\text{sel}}^{(0)} \leftarrow \emptyset$; fit KOH posterior

for $b = 1$ **to** B **do**

$$\boldsymbol{\xi}_{(b)} \leftarrow \arg \max(\min)_{\boldsymbol{\xi} \in \mathcal{D}_{\text{cand}} \setminus \mathcal{D}_{\text{sel}}^{(b-1)}} \text{Crit}(\boldsymbol{\xi}; \text{current posterior}, \mathcal{X}_{\text{pred}})$$

if mode=SDE **then**

No physical experiment; keep current KOH posterior unchanged

else if mode=ADE **then**

Run experiment at $\boldsymbol{\xi}_{(b)}$ to get $\mathbf{y}_{(b)}^{\text{new}}$; augment data; update KOH posterior

end if

$$\mathcal{D}_{\text{sel}}^{(b)} \leftarrow \mathcal{D}_{\text{sel}}^{(b-1)} \cup \{\boldsymbol{\xi}_{(b)}\}$$

end for

return $\mathcal{D}_{\text{sel}}^{(B)}$ and final KOH posterior

2.3 Classical Design Criteria

If the objective is to directly enhance the future predictive performance of the statistical model, particularly the KOH model, only a few prior works have investigated relevant experimental design criteria. In practice, space-filling designs are commonly adopted as an initial exploration and serve as a practical benchmark. Beyond that, the IMSPE minimization criterion is almost the only measure in the existing literature that directly quantifies predictive uncertainty. In addition, here we also compare with the D-optimal criterion in this study, which focuses on improving the estimation of calibration parameters but can also indirectly enhance predictive accuracy. Among these criteria, the D-optimal and IMSPE minimization criteria can actually be formulated and implemented in a fully Bayesian manner, a perspective that has been rarely discussed in previous studies. Their Bayesian formulations are presented in this subsection.

Integrated Mean Squared Prediction Error Minimization The integrated mean squared prediction error (IMSPE) minimization criterion is derived from the I-optimality criterion (Studden, 1977), whose purpose is to maximize the reduction in predictive variance. It was initially proposed by Sacks et al. (1989) as a selection criterion for experimental points that minimize the expected predictive uncertainty over the input space. Subsequently, Leatherman et al. (2017) and Koermer et al. (2024) provided detailed mathematical formulations of IMSPE within the KOH model framework. Here, we briefly outline its underlying principle and discuss its implementation in a fully Bayesian approach.

Based on the predictive covariance matrix given in Equation (6), the Bayesian formulation of the IMSPE criterion in this study is given as

$$\text{IMSPE}(\boldsymbol{\xi}_{(b)}) = \mathbb{E}_{\boldsymbol{\Omega} \sim p(\boldsymbol{\Omega} | \mathbf{y})} \left[\frac{1}{n^*} \text{tr} \left(\boldsymbol{\Sigma}^*(\mathbf{X}^* | \mathbf{y}; \boldsymbol{\Omega}, \mathcal{D}_{\text{sel}}^{(b)}) \right) \right]. \quad (7)$$

where $\text{tr}(\cdot)$ denotes the matrix trace operator. All parameters in the KOH model are bundled into the set $\boldsymbol{\Omega} = (\boldsymbol{\theta}, \boldsymbol{\phi}_1, \boldsymbol{\phi}_2, \sigma^2)$, and $p(\boldsymbol{\Omega} \mid \mathbf{y})$ denotes the posterior distribution. The expectation is taken with respect to the posterior distribution of the model parameters. In practice, the integral is approximated by averaging with equal weights $1/n^*$ over the set of predictive inputs $\mathcal{X}_{\text{pred}}$. We are looking for experimental designs that minimize the IMSPE, which is formally equivalent to choosing

$$\boldsymbol{\xi}_{(b)} = \arg \min_{\boldsymbol{\xi} \in \mathcal{D}_{\text{cand}} \setminus \mathcal{D}_{\text{sel}}^{(b-1)}} \mathbb{E}_{\boldsymbol{\Omega} \sim p(\boldsymbol{\Omega} \mid \mathbf{y})} \left[\frac{1}{n^*} \text{tr} \left(\boldsymbol{\Sigma}^*(\mathbf{X}^* \mid \mathbf{y}; \boldsymbol{\Omega}, \mathcal{D}_{\text{sel}}^{(b)}) \right) \right].$$

In the adaptive (online) design of experiments (ADE), the posterior $p(\boldsymbol{\Omega} \mid \mathbf{y})$ and the observed response \mathbf{y} are both updated at each round b by the newly selected design input $\boldsymbol{\xi}_{(b)}$ and its corresponding field observation $\mathbf{y}_{(b)}^{\text{new}}$.

D-optimality The KOH model framework with two-stage GPs yields a closed-form expression for the response likelihood. Therefore, we can indirectly aim to improve future predictions by selecting experimental designs to better estimate calibration parameters $\boldsymbol{\theta}$. According to Krishna et al. (2021) and Diao et al. (2022), we can first write the Fisher Information Matrix (FIM) of $\boldsymbol{\theta}$ in the usual trace form

$$I_{ij}(\boldsymbol{\theta} \mid \boldsymbol{\Omega}) = \left(\frac{\partial \boldsymbol{\mu}^\top}{\partial \theta_i} \boldsymbol{\Sigma}_{oo}^{-1} \frac{\partial \boldsymbol{\mu}}{\partial \theta_j} + \frac{1}{2} \text{tr} \left(\boldsymbol{\Sigma}_{oo}^{-1} \frac{\partial \boldsymbol{\Sigma}_{oo}}{\partial \theta_i} \boldsymbol{\Sigma}_{oo}^{-1} \frac{\partial \boldsymbol{\Sigma}_{oo}}{\partial \theta_j} \right) \right) \Bigg|_{\boldsymbol{\Omega}}, \quad i, j = 1, \dots, h. \quad (8)$$

Here, $\boldsymbol{\mu}$ and $\boldsymbol{\Sigma}_{oo}$ are involved in Equation (3) and both depend on the parameter set $\boldsymbol{\Omega}$. Thus, the FIM is also conditioned on $\boldsymbol{\Omega}$. In our study, we would like to incorporate the parameter uncertainty, thereby the fully Bayesian FIM is given as

$$I_{ij}(\boldsymbol{\theta}) = \mathbb{E}_{\boldsymbol{\Omega} \sim p(\boldsymbol{\Omega} \mid \mathbf{y})} [I_{ij}(\boldsymbol{\theta} \mid \boldsymbol{\Omega})].$$

The Bayesian D-optimal design is then obtained by maximizing the log-determinant of the FIM, $\text{logdet } I_{ij}(\boldsymbol{\theta})$, after which the corresponding design input is

$$\boldsymbol{\xi}_{(b)} = \arg \max_{\boldsymbol{\xi} \in \mathcal{D}_{\text{cand}} \setminus \mathcal{D}_{\text{sel}}^{(b-1)}} \text{logdet } I_{ij}(\boldsymbol{\theta}).$$

In sequential (offline) design of experiments (SDE), the FIM $I_{ij}(\boldsymbol{\theta})$ can still differ across the candidate design inputs even though the parameter posterior $p(\boldsymbol{\Omega} \mid \mathbf{y})$ is fixed. This is because adding a new experimental input expands the mean vector $\boldsymbol{\mu}$ and the observational block of the covariance matrix $\boldsymbol{\Sigma}_{oo}$, even though the posterior distribution remains unchanged. In adaptive (online) design (ADE), the effect is further amplified since the parameter posterior $p(\boldsymbol{\Omega} \mid \mathbf{y})$ is also updated when a real field response $\mathbf{y}_{(b)}^{\text{new}}$ and a newly selected design input $\boldsymbol{\xi}_{(b)}$ are incorporated.

Maximin Distance Under circumstances where prior information of the model or expert knowledge is not available, space-filling design is commonly adopted (Johnson et al., 1990; Lin and Tang, 2015; Pronzato and Müller, 2012) to seek design points that fill a bounded

experimental region as uniformly as possible. [Johnson et al. \(1990\)](#) proposed the Maximin Distance criterion, which aims to maximize the minimum Euclidean distance between each candidate design point and all previously selected points. In this study, we also use it as a geometric benchmark. The design input is searched in a greedy manner:

$$\boldsymbol{\xi}_{(b)} = \arg \max_{\boldsymbol{\xi} \in \mathcal{D}_{\text{cand}} \setminus \mathcal{D}_{\text{sel}}^{(b-1)}} \min_{\boldsymbol{\xi}_{(j)} \in \mathcal{D}_{\text{sel}}^{(b-1)} (1 \leq j \leq b-1)} \|\boldsymbol{\xi} - \boldsymbol{\xi}_{(j)}\|_2.$$

This criterion promotes the space-filling property of the design without relying on the KOH model or any posterior updates. Therefore, the decision does not depend on whether the design strategy is SDE or ADE.

3 Mutual Information–Based Design Criterion

In this section, we introduce the background of the conventional Bayesian experimental design (BED) framework based on mutual information (MI). Specifically, we first describe how to construct a utility function that guides the selection of experimental inputs to directly improve the predictive distribution $p(\mathbf{y}^*)$ (marginalized over the model parameters $\boldsymbol{\Omega}$). We then incorporate the concept of local complexity of the model prediction and propose a newly hybrid criterion that provides a more efficient search for optimal design locations. Furthermore, we investigate several theoretical properties of the MI-based criterion, including its bias, asymptotic convergence, and its connection to the IMSPE minimization criterion.

3.1 Mutual Information Gain for Improving Future Predictions

From [Lindley \(1972\)](#), the utility function of BED should have the following general form:

$$\begin{aligned} U(\boldsymbol{\xi}) &= \iint u(\boldsymbol{\xi}, \mathbf{y}^{\text{new}}; \boldsymbol{\Omega}) p(\mathbf{y}^{\text{new}}, \boldsymbol{\Omega} \mid \boldsymbol{\xi}) d\boldsymbol{\Omega} d\mathbf{y}^{\text{new}} \\ &= \iint u(\boldsymbol{\xi}, \mathbf{y}^{\text{new}}; \boldsymbol{\Omega}) p(\boldsymbol{\Omega} \mid \mathbf{y}^{\text{new}}, \boldsymbol{\xi}) p(\mathbf{y}^{\text{new}} \mid \boldsymbol{\xi}) d\boldsymbol{\Omega} d\mathbf{y}^{\text{new}}, \end{aligned} \tag{9}$$

where $U(\boldsymbol{\xi})$ is the expected utility of the conditional utility function $u(\boldsymbol{\xi}, \mathbf{y}^{\text{new}}; \boldsymbol{\Omega})$ and \mathbf{y}^{new} represents the (as yet unobserved) outcome of an experiment conducted at $\boldsymbol{\xi}$. Since the true observation is unknown prior to performing the experiment, the expectation is integrated over the joint uncertainty of the model parameters $\boldsymbol{\Omega}$ and the potential observation \mathbf{y}^{new} .

[Ryan et al. \(2016\)](#) introduced the computation of mutual information (MI) between the variable of interest and the potential observation. Consistent with the design objective and sequential design strategy described in Section 2.2, the expected utility at each round b can be expressed as

$$\begin{aligned} U(\boldsymbol{\xi}_{(b)}) &= I(\mathbf{y}^*; \mathbf{y}_{(b)}^{\text{new}} \mid \mathbf{y}, \mathcal{D}_{\text{sel}}^{(b)}) \\ &= \iint p(\mathbf{y}^* \mid \mathbf{y}_{(b)}^{\text{new}}, \mathbf{y}, \mathcal{D}_{\text{sel}}^{(b)}) p(\mathbf{y}_{(b)}^{\text{new}} \mid \mathbf{y}, \mathcal{D}_{\text{sel}}^{(b)}) \\ &\quad \times \log \frac{p(\mathbf{y}^* \mid \mathbf{y}_{(b)}^{\text{new}}, \mathbf{y}, \mathcal{D}_{\text{sel}}^{(b)})}{p(\mathbf{y}^* \mid \mathbf{y}, \mathcal{D}_{\text{sel}}^{(b)})} d\mathbf{y}_{(b)}^{\text{new}} d\mathbf{y}^*. \end{aligned} \tag{10}$$

Corresponding to (9), the marginalized utility function over Ω is defined as the log ratio between the posterior and prior predictive distributions of the quantity of interest:

$$u(\boldsymbol{\xi}_{(b)}, \mathbf{y}_{(b)}^{\text{new}}; \mathbf{y}^*) = \log \frac{p(\mathbf{y}^* | \mathbf{y}_{(b)}^{\text{new}}, \mathbf{y}, \mathcal{D}_{\text{sel}}^{(b)})}{p(\mathbf{y}^* | \mathbf{y}, \mathcal{D}_{\text{sel}}^{(b)})}.$$

We are not the first to propose this utility function. Chaloner and Verdinelli (1995) and Kleingesse and Gutmann (2021) also presented similar formulations, although they either ignored parameter uncertainty or conceptually marginalized it out, thereby not fully capturing how this uncertainty propagates to quantities $\mathbf{y}_{(b)}^{\text{new}}$ and \mathbf{y}^* . In this work, we explicitly expand the marginal distributions to account for the impact of parameter uncertainty on both the potential observation and the future prediction. For computational convenience, we can rewrite Equation (10) as

$$\begin{aligned} U(\boldsymbol{\xi}_{(b)}) &= \iint p(\mathbf{y}^*, \mathbf{y}_{(b)}^{\text{new}} | \mathbf{y}, \mathcal{D}_{\text{sel}}^{(b)}) \\ &\quad \times \log \frac{p(\mathbf{y}^*, \mathbf{y}_{(b)}^{\text{new}} | \mathbf{y}, \mathcal{D}_{\text{sel}}^{(b)})}{p(\mathbf{y}_{(b)}^{\text{new}} | \mathbf{y}, \mathcal{D}_{\text{sel}}^{(b)})p(\mathbf{y}^* | \mathbf{y}, \mathcal{D}_{\text{sel}}^{(b)})} d\mathbf{y}_{(b)}^{\text{new}} d\mathbf{y}^*. \end{aligned} \quad (11)$$

Each marginal likelihood term in both the numerator and denominator of Equation (11) is obtained by integrating over the posterior distribution of the model parameters Ω), e.g.

$$\begin{aligned} p(\mathbf{y}^*, \mathbf{y}_{(b)}^{\text{new}} | \mathbf{y}, \mathcal{D}_{\text{sel}}^{(b)}) &= \int p(\mathbf{y}^*, \mathbf{y}_{(b)}^{\text{new}} | \Omega, \mathcal{D}_{\text{sel}}^{(b)}) p(\Omega | \mathbf{y}) d\Omega, \\ p(\mathbf{y}_{(b)}^{\text{new}} | \mathbf{y}, \mathcal{D}_{\text{sel}}^{(b)}) &= \int p(\mathbf{y}_{(b)}^{\text{new}} | \Omega, \mathcal{D}_{\text{sel}}^{(b)}) p(\Omega | \mathbf{y}) d\Omega, \\ p(\mathbf{y}^* | \mathbf{y}, \mathcal{D}_{\text{sel}}^{(b)}) &= \int p(\mathbf{y}^* | \Omega, \mathcal{D}_{\text{sel}}^{(b)}) p(\Omega | \mathbf{y}) d\Omega. \end{aligned}$$

In the adaptive (online) design of experiments (ADE), the posterior $p(\Omega | \mathbf{y})$ and the observed response \mathbf{y} are both updated or appended at each round b . Considering both parameter uncertainty and predictive uncertainty, this utility function can be interpreted as the expected Kullback-Leibler (KL) divergence (Kullback and Leibler, 1951) between the posterior predictive and prior predictive distributions of future observations \mathbf{y}^* , integrated over all possible model parameters Ω . Hence, the design input can be selected by maximizing the expected utility

$$\boldsymbol{\xi}_{(b)} = \arg \max_{\boldsymbol{\xi} \in \mathcal{D}_{\text{cand}} \setminus \mathcal{D}_{\text{sel}}^{(b-1)}} U(\boldsymbol{\xi}).$$

Figure 1 shows an illustrative example of the evolution of the joint predictive distribution at two locations over a 5-run sequential (offline) design of experiments (SDE) using this proposed criterion. We can see from the plot that, as the design rounds progress, the uncertainty of the distribution decreases substantially and the posterior density (95% Highest Posterior Density (HPD)) is becoming more sharply focused around the true value.

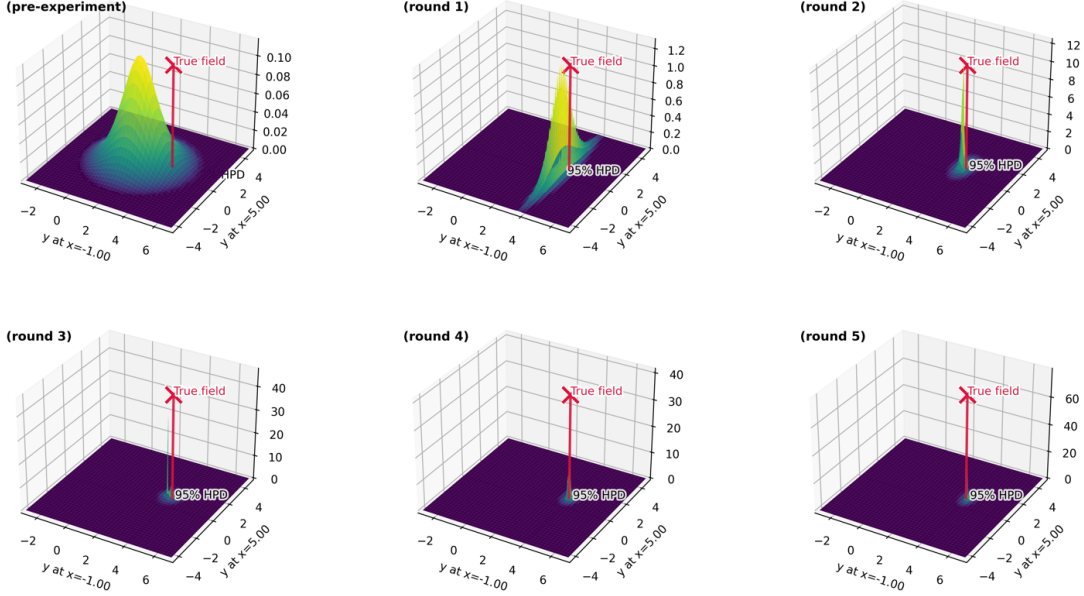


Figure 1: Evolution of the joint predictive distribution at two locations under a 5-run sequential (offline) design of experiments (SDE) using the proposed MI-based criterion.

3.2 Hybrid Criterion with Local Complexity Adjustment

The criterion based on mutual information gain proposed above can help obtain the points that yield the greatest reduction in global predictive uncertainty. However, this criterion may also have the drawback of oversampling in regions of high predictive variance and missing critical model structure such as extrema or inflection regions. Inspired by numerical optimization methods such as Newton’s method (Bonnans et al., 2006), we propose to quantify the local complexity of the predictive surface through a composite metric that combines the local slope and the slope-variation at the candidate input $\xi_{(b)}$.

Let the predictive mean function at a single candidate input $\xi_{(b)} \in \mathbb{R}^d$ be expressed as $\mu^*(\xi_{(b)}) \in \mathbb{R}^p$, where p denotes the number of output dimensions (tasks). In a fully Bayesian way it can be written as

$$\mu^*(\xi_{(b)}) = \mathbb{E}_{\Omega \sim p(\Omega|y)} [\mu^*(\xi_{(b)}; \Omega)].$$

The local slope at $\xi_{(b)}$ is then characterized by the Jacobian matrix

$$\mathbf{J}(\xi_{(b)}) = \frac{\partial \mu^*(\xi_{(b)})}{\partial \xi_{(b)}} \in \mathbb{R}^{p \times d},$$

whose Frobenius norm quantifies the overall rate of change of the predictive mean field with respect to the input dimensions:

$$g(\xi_{(b)}) = \|\mathbf{J}(\xi_{(b)})\|_F = \sqrt{\sum_{i=1}^p \sum_{j=1}^d \left(\frac{\partial \mu_i^*(\xi_{(b)})}{\partial \xi_{(b),j}} \right)^2}, \quad (12)$$

where $\xi_{(b)} = (\xi_{(b),1}, \xi_{(b),2}, \dots, \xi_{(b),d})^\top$. In practice, we flatten all outputs into a single vector so that the multi-task case can be treated as a single-output scenario and Frobenius norm

provides a natural scalar measure of local sensitivity without requiring task-specific weights. The scalar quantity $g(\boldsymbol{\xi}_{(b)})$ serves as a measure of the local slope or steepness of the predictive mean field, and forms the first component of our composite local complexity metric.

The other component of the metric evaluates the change rate of the local slope. In continuous optimization problems, this can be conveniently quantified using curvature. However, in the context of physical experimental design, where the budget is normally limited and the candidate design inputs are highly discrete, it is impractical to compute smooth derivatives. Therefore, we construct a slope-change score that measures the total variation of the local slope among all discrete candidate points. Specifically, we define it as

$$s(\boldsymbol{\xi}_{(b)}) = \frac{1}{k} \sum_{j \in \mathcal{N}(b)} |g(\boldsymbol{\xi}_{(b)}) - g(\boldsymbol{\xi}_{(j)})|, \quad (13)$$

where $\mathcal{N}(b)$ denotes the index set of the k nearest neighbors of $\boldsymbol{\xi}_{(b)}$ in the input space. This formulation can be interpreted as a discrete analogue of curvature, measuring how rapidly the local slope changes in the neighborhood of each candidate $\boldsymbol{\xi}_{(b)}$. A larger $s(\boldsymbol{\xi}_{(b)})$ indicates a region with higher nonlinearity or stronger local variation.

For the computation of Equation (12), either automatic differentiation or the finite-difference method can be employed. After obtaining both the slope $g(\boldsymbol{\xi}_{(b)})$ from Equation (12) and the slope-change score $s(\boldsymbol{\xi}_{(b)})$ from Equation (13), we standardize them to the $[0, 1]$ range and give the local complexity measurement as a weighted combination of these two components:

$$C(\boldsymbol{\xi}_{(b)}) = w_g \tilde{g}(\boldsymbol{\xi}_{(b)}) + w_s \tilde{s}(\boldsymbol{\xi}_{(b)}), \quad w_g + w_s = 1,$$

where $\tilde{g}(\cdot)$ and $\tilde{s}(\cdot)$ denote the normalized slope and slope-change score, respectively. The weights w_g and w_s can be freely chosen according to prior knowledge about the model behavior or different design preferences. For example, a larger w_g places more emphasis on regions of steep gradients, while a larger w_s encourages exploration of regions exhibiting strong nonlinearity or fluctuation. This composite score $C(\boldsymbol{\xi}_{(b)})$ therefore offers a flexible and interpretable metric for quantifying the local complexity of the model.

If we hybridize the proposed local complexity adjustment with criteria driven by uncertainty reduction, then we comprehensively account for the global predictive uncertainty as well as the local structural pattern of the predictive surface. Specifically, we can incorporate the local complexity term with both the MI-based utility in Equation (11) and the IMSPE in Equation (7). The formulations of each are given by:

$$U_{\text{hyb}}^{\text{MI}}(\boldsymbol{\xi}_{(b)}) = (1 - \alpha) U(\boldsymbol{\xi}_{(b)}) + \alpha C(\boldsymbol{\xi}_{(b)}), \quad \alpha \in [0, 1], \quad (14)$$

$$U_{\text{hyb}}^{\text{IMSPE}}(\boldsymbol{\xi}_{(b)}) = (1 - \alpha) [-\text{IMSPE}(\boldsymbol{\xi}_{(b)})] + \alpha C(\boldsymbol{\xi}_{(b)}), \quad \alpha \in [0, 1]. \quad (15)$$

The weighting factor α is also user-chosen to balance the design preference between predictive uncertainty and the local pattern of the predictive surface.

3.3 Theoretical Properties

In Section 2.3, we discussed the IMSPE minimization criterion, which has a close resemblance, in terms of function, to the MI-based criterion defined in Equation (10), as both aim

to directly reduce predictive uncertainty. It is therefore theoretically valuable to formalize the connection between these two design objectives. For theoretical clarity, we first establish the relationship conditional on the model parameters Ω . Since the Bayesian design criteria considered in this work marginalize over Ω through the posterior distribution $p(\Omega \mid \mathbf{y})$, the conditional result can be interpreted as describing the local behavior of the integrand within the Bayesian expectation. In a myopic sequential or adaptive design framework, the selection of the design point $\xi_{(b)}$ at round b depends on the posterior state obtained after the previous selection $\xi_{(b-1)}$. The MI-based criterion can be interpreted as quantifying the change in predictive entropy before and after the inclusion of the new observation $\mathbf{y}_{(b)}^{\text{new}}$ at $\xi_{(b)}$. While the IMSPE minimization is formulated in terms of the predictive variance at the current round b , it implicitly measures the reduction in predictive variance relative to the variance obtained from the previous design history $\mathcal{D}_{\text{sel}}^{(b-1)}$ without choosing $\xi_{(b)}$. Building on this, we can provide a general relationship showing that the MI-based criterion is locally asymptotically equivalent to the IMSPE minimization criterion as the sequential design proceeds. We may further interpret the IMSPE minimization criterion as a relaxed form of the MI-based criterion. It preserves the same optimization direction but provides a computationally simpler surrogate, since the IMSPE depends only on the second moment (trace) of the predictive covariance rather than the full covariance structure. Before proceeding with the formal expression, we denote $\Sigma_{(b-1)}^*$ as the pre-experiment predictive covariance matrix at round $b-1$, corresponding to the part $\Sigma^* \mid \mathbf{y}; \Omega, \mathcal{D}_{\text{sel}}^{(b-1)}$ in Equation (7). Similarly, $\Sigma_{(b)}^*$ denotes the corresponding predictive covariance matrix at round b . Let $\lambda_{\min}(\Sigma_{(b-1)}^*)$ and $\lambda_{\max}(\Sigma_{(b-1)}^*)$ denote the smallest and the biggest eigenvalue of $\Sigma_{(b-1)}^*$, respectively. Then, we have the following theorem:

Theorem 1 (Local asymptotic relationship between MI and IMSPE). *Assume that, (i) conditional on Ω , $(\mathbf{y}^*, \mathbf{y}_{(b)}^{\text{new}})$ is jointly Gaussian, (ii) $\Sigma_{(b-1)}^*$ is symmetric positive definite with eigenvalues $0 < \lambda_{\min} \leq \lambda_{\max} < \infty$. Define the covariance reduction and IMSPE reduction at round b as*

$$\Delta \Sigma^*(\xi_{(b)}) := \Sigma_{(b-1)}^* - \Sigma_{(b)}^* \succeq \mathbf{0}, \quad \Delta \text{IMSPE}(\xi_{(b)} \mid \Omega) := \frac{1}{n^*} \text{tr}(\Delta \Sigma^*(\xi_{(b)})),$$

As the sequential design rounds proceed, the following small-update regime holds:

$$\left\| (\Sigma_{(b-1)}^*)^{-1/2} \Delta \Sigma^*(\xi_{(b)}) (\Sigma_{(b-1)}^*)^{-1/2} \right\|_2 \rightarrow 0.$$

Then there exists a finite constant C_{b-1} , depending on $\Sigma_{(b-1)}^*$, such that

$$\frac{U(\xi_{(b)} \mid \Omega)}{\Delta \text{IMSPE}(\xi_{(b)} \mid \Omega)} \rightarrow C_{b-1} \quad \text{as} \quad \Delta \Sigma^*(\xi_{(b)}) \rightarrow \mathbf{0},$$

and this constant is bounded in terms of the eigenvalues of $\Sigma_{(b-1)}^*$:

$$\frac{n^*}{2 \lambda_{\max}(\Sigma_{(b-1)}^*)} \leq C_{b-1} \leq \frac{n^*}{2 \lambda_{\min}(\Sigma_{(b-1)}^*)}.$$

Proof. See Appendix A. □

This result establishes a quantitative link between the two prediction-improvement criteria. At each design round, the new chosen location $\boldsymbol{\xi}_{(b)}$ and the new observation $\mathbf{y}_{(b)}^{\text{new}}$ (if in ADE) bring a reduction to predictive covariance. As the rounds proceed sequentially and b becomes sufficiently large, maximizing mutual information becomes asymptotically equivalent to minimizing the IMSPE, with their difference collapsing to a ratio factor only related to the current predictive uncertainty structure. This ratio factor can be stable as the predictive covariance matrix becomes approximately isotropic as the design rounds continue, leading to the limiting equivalence established in Theorem 1. The theorem is stated conditional on the model parameters $\boldsymbol{\Omega}$, however, the Bayesian design criterion marginalizes over $\boldsymbol{\Omega}$ through the posterior $p(\boldsymbol{\Omega} \mid \mathbf{y})$. As the sequential design progresses, the posterior update of $\boldsymbol{\Omega}$ also becomes increasingly small, i.e., $p(\boldsymbol{\Omega} \mid \mathbf{y}_{1:b}) - p(\boldsymbol{\Omega} \mid \mathbf{y}_{1:b-1}) \rightarrow 0$, the conditional asymptotic equivalence extends naturally to the Bayesian (marginalized) setting.

From another perspective, the MI-based criterion can be interpreted as a spectrally weighted version of IMSPE. In early design stages, when b is relatively small and predictive uncertainty is highly anisotropic, the MI-based criterion is more sensitive to the directions associated with larger uncertainty reduction and it can guide experimental design more effectively especially at early rounds. Therefore, the MI-based criterion can be regarded as a generalization of the IMSPE criterion, providing enhanced robustness and exploration ability. This is more aligned with the Bayesian experimental design framework because it explicitly considers the full structure of predictive covariance throughout the process.

For the computation of mutual information gain in Equation (11), due to the intractability of the marginal likelihood of \mathbf{y}^* and $\mathbf{y}_{(b)}^{\text{new}}$ both individually and jointly—as well as the posterior $p(\boldsymbol{\Omega} \mid \mathbf{y})$, the conventional Monte Carlo (MC) estimator cannot be directly applied. Instead, a nested Monte Carlo (NMC) estimator (Rainforth et al., 2018) is required. In particular, (11) can be computed as an NMC estimator:

$$\widehat{U}_{S,J}(\boldsymbol{\xi}_{(b)}) = \frac{1}{S} \sum_{s=1}^S \left[\log \widehat{p}_J^{\text{joint}}(\mathbf{y}_s^*, \mathbf{y}_{(b),s}^{\text{new}}) - \log \widehat{p}_J^*(\mathbf{y}_s^*) - \log \widehat{p}_J^{\text{new}}(\mathbf{y}_{(b),s}^{\text{new}}) \right]. \quad (16)$$

Let $S \in \mathbb{N}$ be the number of outer samples and $J \in \mathbb{N}$ the number of inner samples. For each outer index $s = 1, \dots, S$, we first draw $\boldsymbol{\Omega}_s^{(0)} \sim p(\boldsymbol{\Omega} \mid \mathbf{y}, \mathcal{D}_{\text{sel}}^{(b)})$ and then sample $(\mathbf{y}_s^*, \mathbf{y}_{(b),s}^{\text{new}}) \sim p(\mathbf{y}_s^*, \mathbf{y}_{(b),s}^{\text{new}} \mid \mathbf{y}, \boldsymbol{\Omega}_s^{(0)}, \mathcal{D}_{\text{sel}}^{(b)})$. In the inner layer, we independently draw $\boldsymbol{\Omega}_s^{(1:J)} = \{\boldsymbol{\Omega}_s^{(j)}\}_{j=1}^J$ i.i.d. from $p(\boldsymbol{\Omega} \mid \mathbf{y})$. The Monte Carlo estimates of each corresponding marginal density in Equation (16) for each outer sample s can then be expressed as

$$\begin{aligned} \widehat{p}_J^{\text{joint}}(\mathbf{y}_s^*, \mathbf{y}_{(b),s}^{\text{new}}) &= \frac{1}{J} \sum_{j=1}^J p(\mathbf{y}_s^*, \mathbf{y}_{(b),s}^{\text{new}} \mid \boldsymbol{\Omega}_s^{(j)}, \mathcal{D}_{\text{sel}}^{(b)}), \\ \widehat{p}_J^*(\mathbf{y}_s^*) &= \frac{1}{J} \sum_{j=1}^J p(\mathbf{y}_s^* \mid \boldsymbol{\Omega}_s^{(j)}, \mathcal{D}_{\text{sel}}^{(b)}), \\ \widehat{p}_J^{\text{new}}(\mathbf{y}_{(b),s}^{\text{new}}) &= \frac{1}{J} \sum_{j=1}^J p(\mathbf{y}_{(b),s}^{\text{new}} \mid \boldsymbol{\Omega}_s^{(j)}, \mathcal{D}_{\text{sel}}^{(b)}). \end{aligned}$$

We now examine the asymptotic behavior of the proposed NMC estimator $\widehat{U}_{S,J}(\boldsymbol{\xi}_{(b)})$ towards $U(\boldsymbol{\xi}_{(b)})$ as the number of samples increases. From [Hong and Juneja \(2009\)](#), if the outer-layer transformation/function is thrice differentiable with bounded third derivative, then the estimator can achieve a convergence rate of $O(1/S + 1/J^2)$. Here in our setting, the transformation is $f(\cdot) = \log(\cdot)$, thus it satisfies these smoothness conditions on any compact subset $[\tau, \infty) \subset \mathbb{R}_+$, as summarized in the lemma below.

Lemma 1 (Smoothness and bounded derivatives of the outer-layer function). *Let the outer-layer function of the proposed NMC estimator be the log function $f : \mathbb{R}_+ \rightarrow \mathbb{R}$, $x \mapsto \log(x)$. Let the argument of f be lower-bounded by a sufficiently small positive constant $\tau > 0$, i.e., f is only evaluated for inputs in $[\tau, \infty)$. Then f is thrice differentiable continuously on $[\tau, \infty)$, and all derivatives up to order three are bounded.*

Proof. See [Appendix A](#). □

Following [Lemma 1](#), our MI-based utility function can be viewed as a specific instance of the general nested expectation problem analyzed by [Hong and Juneja \(2009\)](#). Therefore, the NMC estimator in [Equation \(16\)](#) satisfies the established convergence properties, with the mean square error of $\widehat{U}_{S,J}(\boldsymbol{\xi}_{(b)})$ decaying at a rate of $O(1/S + 1/J^2)$.

Corollary 1 (Convergence of the NMC estimator). *Under the conditions in [Lemma 1](#) and assuming independence between the inner and outer samplers, the mean squared error of $\widehat{U}_{S,J}(\boldsymbol{\xi}_{(b)})$ converges to 0 at rate $O(S^{-1} + J^{-2})$,*

$$\mathbb{E}[(\widehat{U}_{S,J}(\boldsymbol{\xi}_{(b)}) - U(\boldsymbol{\xi}_{(b)}))^2] = O(S^{-1} + J^{-2}).$$

Proof. See [Appendix A](#). □

If the total computational budget is $T = S \times J$, [Rainforth et al. \(2018\)](#) showed that the NMC estimator can achieve its optimal convergence rate of the tightest bound $O(T^{-2/3})$ when the inner sample size J is proportional to S^2 . It is also known that the NMC estimator is biased for any finite J , while increasing the outer sample size $S \rightarrow \infty$ can merely eliminate the variance. However, if $J \rightarrow \infty$ additionally, the NMC estimator in our work converges almost surely to the true utility value because the bias term is also eliminated.

Corollary 2 (Bias and almost sure convergence of the NMC estimator). *For any finite S, J , $\widehat{U}_{S,J}(\boldsymbol{\xi}_{(b)})$ is a biased estimator of $U(\boldsymbol{\xi}_{(b)})$, i.e.,*

$$\mathbb{E}[\widehat{U}_{S,J}(\boldsymbol{\xi}_{(b)})] \neq U(\boldsymbol{\xi}_{(b)}).$$

Under the regularity conditions of [Lemma 1](#), if $J \rightarrow \infty$ and $S \rightarrow \infty$, then $\widehat{U}_{S,J}(\boldsymbol{\xi}_{(b)})$ converges to $U(\boldsymbol{\xi}_{(b)})$ almost surely:

$$\widehat{U}_{S,J}(\boldsymbol{\xi}_{(b)}) \xrightarrow{a.s.} U(\boldsymbol{\xi}_{(b)}).$$

Proof. See [Appendix A](#). □

4 Computation Strategies

After discussing the proposed MI-based criterion in Section 3.1 and the classical criteria in Section 2.3, we now present several computational strategies aimed at reducing the overall computational cost and demonstrating the resulting efficiency gains.

In Section 3.3, we discussed that the computational burden of the NMC estimator for the MI-based criterion is substantial as it requires two layers of discretized integration. Specifically, we sample the predictive response \mathbf{y}^* and $\mathbf{y}_{(b)}^{\text{new}}$ as well as the model parameters $\boldsymbol{\Omega}$ in order to consider all sources of uncertainty. The outer sample size S primarily determines the magnitude of the predictive variance and typically depends on the dimensionality of the conditional Gaussian distribution $p(\mathbf{y}_s^*, \mathbf{y}_{(b),s}^{\text{new}} \mid \boldsymbol{\Omega}_s^{(j)}, \mathcal{D}_{\text{sel}}^{(b)})$. According to Corollary 1 and Corollary 2, the estimate $\widehat{U}_{S,J}(\boldsymbol{\xi}_{(b)})$ becomes accurate as $J \rightarrow \infty$ and $S \rightarrow \infty$. When using experimental design criteria based on computing the covariance matrix, reducing S is generally impractical, as doing so would inevitably result in high Monte Carlo variance and unstable design decisions. In contrast, the required inner sample size J largely depends on the complexity of the posterior distribution $p(\boldsymbol{\Omega} \mid \mathbf{y})$. Thus, it is more desirable to reduce J , which corresponds to constructing a refined approximation using fewer components in the associated Gaussian mixture, even though this procedure may introduce some extra bias, depending on how much representational capacity is retained. Other than existing approaches that use the variational lower bounds to approximate the real EIG by stochastic gradient descent (Foster et al., 2019, 2020; Kleinegesse and Gutmann, 2021), our method is motivated by Runnalls’ algorithm (Runnalls, 2007) and clustering-based reduction methods (Schieferdecker and Huber, 2009). We mitigate the computational cost by compressing the Gaussian mixture, which is the inner layer of the NMC estimator in Equation (16), enabling a substantial reduction in computational cost while preserving the representational capacity as much as possible.

In Algorithm 1, if we perform online adaptive design of experiments (ADE), the posterior distribution $p(\boldsymbol{\Omega} \mid \mathbf{y})$ must be updated after each experiment by appending the newly observed response $\mathbf{y}_{(b)}^{\text{new}}$ to the existing data \mathbf{y} . Consequently, the predictive quantities $\boldsymbol{\mu}^*$ and $\boldsymbol{\Sigma}^*$ in Equation (6) must also be updated at every round. In contrast, under offline sequential design of experiments (SDE), the parameter posterior remains fixed because no real experiments are performed during the design stage. Thus, the predictive mean $\boldsymbol{\mu}^*$ remains unchanged across rounds. However, the predictive covariance $\boldsymbol{\Sigma}^*$ still varies because the covariance structure depends not only on the parameters $\boldsymbol{\Omega}$ but also on the relative positions of the inputs. Therefore, for criteria involving covariance computations, such as IMSPE minimization, D-optimality, and mutual information gain, the naive implementation would require recomputing the predictive covariance from scratch at each round. To address this issue and accelerate the SDE process, we precompute and cache the full covariance matrix in the beginning, and then apply the Schur complement updates to obtain the predictive covariance efficiently.

4.1 Gaussian Mixture Compression

We first briefly overview Runnalls’ algorithm. Runnalls’ method (Runnalls, 2007) reduced the Gaussian mixture model (GMM) by greedily pruning or merging components so

as to minimize the increase in Kullback-Leibler (KL) divergence. At each iteration, the algorithm evaluates and compares the divergence for all candidate pairs, merges the optimal pair via moment matching, and repeats this process until the desired number of components is reached. It is commonly used as an initiation for mixture reduction. In addition, the k -means algorithm (Lloyd, 1982) is a classical clustering method frequently employed for classifying high-dimensional data. Unlike the approach of Schieferdecker and Huber (2009), which first applies Runnalls’ algorithm, then performs k -means clustering, followed by a refinement step, our method is more appropriate to high-dimensional Gaussian mixtures. Because the predictive outputs often involve dozens or even hundreds of locations, it is essential to normalize the component means before performing clustering. As the first step, we whiten the conditional prediction using the Cholesky decomposition of

$$\Sigma_{\text{avg}}^* = \mathbb{E}[\Sigma_j^*] + \text{Cov}(\boldsymbol{\mu}_j^*), \quad j = 1, \dots, J$$

which can be interpreted as a combination of the average covariance and the dispersion of the predictive means. This measure ensures that all directions are scaled comparably, and thus Euclidean distances in the transformed space more faithfully reflect Mahalanobis distances. For simplicity, we omit the outer sample index here and denote the whitened means \mathbf{u}_j^* by

$$\mathbf{u}_j^* = \mathbf{L}^{-1}(\boldsymbol{\mu}_j^* - \bar{\boldsymbol{\mu}}^*), \quad \mathbf{L}\mathbf{L}^\top = \Sigma_{\text{avg}}^*, \quad j = 1, \dots, J.$$

In the second step, we apply k -means clustering in this whitened space to compress the original J components into an initially smaller representation with J_0 clusters. For each cluster, moment matching (mean and covariance) is performed to obtain a reduced GMM with J_0 components. Each component is characterized by a new mean $\boldsymbol{\mu}_k^*$, covariance Σ_k^* , and weight π_k^* ($k = 1, \dots, J_0$, $\pi_k \geq 0$, $\sum_k \pi_k = 1$).

Next, we refine the mixture of J_0 initial clusters by applying a greedy Runnalls’ algorithm to further reduce the number of components to a target value J_{target} . To improve stability and reduce computational overhead, we precompute the Cholesky factors and log-determinants of all covariance matrices prior to this step. The loss function is based on the KL divergence, and in our case is given as

$$D_{ij} = \frac{1}{2} \left[(\pi_i + \pi_j) \log |\Sigma_{ij}^*| - \pi_i \log |\Sigma_i^*| - \pi_j \log |\Sigma_j^*| \right].$$

where Σ_{ij}^* is the covariance matrix obtained via moment matching between components i and j among J_0 components. However, computing moment matching for all pairwise combinations (random pairing) requires $O(J_0^2)$ operations, which could be very expensive in practice because complex posterior distributions usually require very large sample sizes J and hence large J_0 . To overcome this limitation, we consider a key innovation: using K -nearest neighbors (KNN) (Cover and Hart, 1967) to restrict candidate merging pairs. After whitening, the scales across different directions become consistent, and the Euclidean distance between two Gaussian distributions becomes more aligned with a Mahalanobis geometry. Consequently, the nearest neighbors of a component are almost always the most promising candidates for merging, which avoids unnecessary global pairwise comparisons. By selecting nn_k nearest neighbors per component, the computational complexity is reduced from $O(J_0^2)$ to $O(J_0 \times nn_k)$ and the reduced mixture still retains the strong representational capacity of the original GMM. The process is summarized in Algorithm 2.

Algorithm 2 Gaussian Mixture Compression with Whitening, k -means Initialization, and KNN-Guided Runnalls

Require: Original mixture $\{(\pi_j, \boldsymbol{\mu}_j^*, \boldsymbol{\Sigma}_j^*)\}_{j=1}^J$ (equal weights in MCMC case: $\pi_j = 1/J$); final target size J_{target} ; initial cluster size J_0 ; KNN size nn_k ; refresh period r

Ensure: Compressed mixture $\{(\pi_k^*, \boldsymbol{\mu}_k^*, \boldsymbol{\Sigma}_k^*)\}_{k=1}^{J_{\text{target}}}$

Whitening. Compute $\bar{\boldsymbol{\mu}}^* = \frac{1}{J} \sum_j \boldsymbol{\mu}_j^*$ and $\boldsymbol{\Sigma}_{\text{avg}}^* \approx \frac{1}{J} \sum_j \boldsymbol{\Sigma}_j^* + \frac{1}{J} \sum_j (\boldsymbol{\mu}_j^* - \bar{\boldsymbol{\mu}}^*)(\boldsymbol{\mu}_j^* - \bar{\boldsymbol{\mu}}^*)^\top$. Cholesky decomposition: $\mathbf{L}\mathbf{L}^\top = \boldsymbol{\Sigma}_{\text{avg}}^*$. Whiten means: $\mathbf{u}_j^* = \mathbf{L}^{-1}(\boldsymbol{\mu}_j^* - \bar{\boldsymbol{\mu}}^*)$.

k -means compression. Run weighted k -means on $\{\mathbf{u}_j^*\}$ to obtain J_0 clusters; for each cluster perform moment matching to form new components $\{(\pi_k^*, \boldsymbol{\mu}_k^*, \boldsymbol{\Sigma}_k^*)\}_{k=1}^{J_0}$.

KNN construction. Re-whiten the J_0 new components obtained from the last stage and build KNN neighborhoods of size nn_k .

KL-based merging. For each KNN pair (i, j) use Runnalls' algorithm based on

$$D_{ij} = \frac{1}{2} [(\pi_i^* + \pi_j^*) \log |\boldsymbol{\Sigma}_{ij}^*| - \pi_i^* \log |\boldsymbol{\Sigma}_i^*| - \pi_j^* \log |\boldsymbol{\Sigma}_j^*|].$$

After it, we obtain the moment-matched merge $(\pi_{ij}^*, \boldsymbol{\mu}_{ij}^*, \boldsymbol{\Sigma}_{ij}^*)$.

while $J_0 > J_{\text{target}}$ **do**

 Evaluate D_{ij} over KNN pairs and merge $(i, j) = \arg \min D_{ij}$.

 Update $(\pi_k^*, \boldsymbol{\mu}_k^*, \boldsymbol{\Sigma}_k^*)$ using moment matching.

 Every r merges: re-whiten and rebuild the KNN neighborhoods.

end while

return Final compressed mixture $\{(\pi_k^*, \boldsymbol{\mu}_k^*, \boldsymbol{\Sigma}_k^*)\}_{k=1}^{J_{\text{target}}}$.

4.2 Precomputation and Schur Complement

We consider the enlarged covariance structure after the first b design points have been selected. Then, unlike the original full covariance matrix in Equation (4), the updated one at round b is

$$\text{Cov} \left[\begin{pmatrix} \mathbf{y}^* \\ \mathbf{y}_{(1:b)}^{\text{new}} \\ \mathbf{y} \end{pmatrix} \right] = \begin{pmatrix} \boldsymbol{\Sigma}_{**} & \boldsymbol{\Sigma}_{*(\text{new}, 1:b)} & \boldsymbol{\Sigma}_{*o} \\ \boldsymbol{\Sigma}_{(\text{new}, 1:b)*} & \boldsymbol{\Sigma}_{(\text{new}, 1:b)(\text{new}, 1:b)} & \boldsymbol{\Sigma}_{(\text{new}, 1:b)o} \\ \boldsymbol{\Sigma}_{o*} & \boldsymbol{\Sigma}_{o(\text{new}, 1:b)} & \boldsymbol{\Sigma}_{oo} \end{pmatrix} \in \mathbb{R}^{(n^*+N_o) \times (n^*+N_o)},$$

where $N_o = n + m + b$ and we can extract the observational block portion out of this matrix and define it by

$$\boldsymbol{\Sigma}_{oo}^{(b)} := \begin{pmatrix} \boldsymbol{\Sigma}_{(\text{new}, 1:b)(\text{new}, 1:b)} & \boldsymbol{\Sigma}_{(\text{new}, 1:b)o} \\ \boldsymbol{\Sigma}_{o(\text{new}, 1:b)} & \boldsymbol{\Sigma}_{oo} \end{pmatrix} \in \mathbb{R}^{N_o \times N_o}.$$

For the IMSPE minimization criterion and MI-based criterion, the core part of computation involves evaluating the predictive covariance $\boldsymbol{\Sigma}^*$ via Equation (6). Inside this formula, we can recognize the computational bottleneck is the inversion of the observation block $\boldsymbol{\Sigma}_{oo}^{(b)}$. In the sequential experimental design, $\boldsymbol{\Sigma}_{oo}^{(b)}$ expands to $\boldsymbol{\Sigma}_{oo}^{(b+1)}$ and must in principle be inverted at every round, resulting in substantial computational cost.

If we directly rely on Gaussian process prediction APIs to compute $\boldsymbol{\Sigma}^*$, we have to reconstruct and invert the enlarged kernel matrix at each round. For each $\boldsymbol{\Omega}_s^{(j)}$, each round b and each candidate design point $\boldsymbol{\xi} \in \mathcal{D}_{\text{cand}} \setminus \mathcal{D}_{\text{sel}}^{(b-1)}$, the computational complexity therefore is

$$O(N_o^3 + N_o^2 n^* + N_o n^{*2}),$$

where N_o^3 stands for Cholesky decomposition of $\boldsymbol{\Sigma}_{oo}^{(b)}$ and the other two terms correspond to two triangular solves, thus the final complexity is dominated by the relative sizes of N_o and n^* .

To reduce this computational burden, we propose a method that first precomputes the full covariance matrix over all observations, candidate points, and prediction inputs. At each round, the corresponding submatrix required by the criterion is then obtained by slicing the precomputed kernel matrix according to the selected design location. In this way, all covariance blocks needed can be obtained via inexpensive slicing instead of recomputation. Since the covariance structure expands by adding one input at each round, we apply the efficient Schur complement together with a rank-one update (Sherman and Morrison, 1950) to update the required matrices. This avoids recomputing the full inverse $(\boldsymbol{\Sigma}_{oo}^{(b)})^{-1}$ at each round as well as the corresponding predictive covariance $\boldsymbol{\Sigma}_{(b)}^*$. As a result, the computational complexity is decreased from cubic to quadratic, being

$$O(N_o^2 + N_o n^* + n^{*2}),$$

and similarly the complexity is dominated by the relative sizes of N_o and n^* . The computational details can be seen in Appendix B.

4.3 Overall Computational Complexity

We now summarize the overall computational savings in evaluating the predictive covariance Σ^* in a fully Bayesian approach, achieved by combining the Gaussian mixture compression in Section 4.1 with the precomputation and Schur complement strategy in Section 4.2.

Firstly, let us figure out the total evaluations over all candidate design points in $\mathcal{D}_{\text{cand}}$ across the budget B rounds in SDE. The set $\mathcal{D}_{\text{cand}}$ contains M initial candidates. Let $\mathcal{D}_{\text{sel}}^{(b-1)}$ denote the set of selected design points after $(b-1)$ rounds. At round b , the number of remaining candidates is

$$M_b = |\mathcal{D}_{\text{cand}} \setminus \mathcal{D}_{\text{sel}}^{(b-1)}| = M - (b - 1).$$

Hence, the total number of scans over the entire sequential design can be expressed by

$$\sum_{b=1}^B M_b = \sum_{b=1}^B (M - b + 1) = MB - \frac{B(B-1)}{2}.$$

For notational brevity, we let the complexity of this part be $O(BM)$.

Naive baseline. If we compute $\Sigma_{(b)}^*$ without any compression or precomputation, the naive overall complexity can therefore be given as

$$O\left(J \times \underbrace{BM}_{\text{total candidates over all rounds}} \times (N_o^3 + N_o^2 n^* + N_o n^{*2})\right).$$

After improvement. Combining both improvements in Section 4.1 and Section 4.2, the overall complexity becomes

$$O\left(J_{\text{target}} \times \underbrace{BM}_{\text{total candidates over all rounds}} \times (N_o^2 + N_o n^* + n^{*2})\right).$$

In comparison, it is evident that combining the two strategies yields substantial computational savings, especially for the efficiency of the MI-based, IMSPE minimization and D-optimal criteria.

Complexity of different design criteria. Having established the cost of computing the predictive covariance Σ^* in the fully Bayesian setting, we now turn to the three design criteria introduced earlier. These three all depend on the computation of the covariance matrix but differ in additional work due to their respective utility functions.

1. **Mutual information (MI) gain:** The MI-based criterion requires S outer samplers to compute the log-density of a joint Gaussian distribution of dimension $(n^* + 1)$ and J_{target} Gaussian mixture components. Each Gaussian log-density evaluation requires only one triangular solve and one quadratic form, thus the complexity is $O((n^* + 1)^2)$. Therefore, the total complexity for the MI criterion becomes

$$O\left(J_{\text{target}} \times BM \times (N_o^2 + N_o n^* + n^{*2}) + S \times J_{\text{target}} \times BM \times (n^* + 1)^2\right),$$

assuming that one new design input is selected at each round.

2. **IMSPE minimization:** Compared with MI, the IMSPE minimization criterion in the Bayesian setting only requires computing the trace of $\Sigma_{(b)}^*$ for each $\Omega^{(j)}$ sample and does not involve the outer S -loop. It is already computationally efficient, but with our Gaussian mixture compression strategy, the overall complexity reduces to

$$O\left(J_{\text{target}} \times BM \times (N_o^2 + N_o n^* + n^{*2})\right).$$

3. **D-optimality:** The fully Bayesian D-optimal criterion is different from the two criteria above in that it relies primarily on the observation covariance block $\Sigma_{oo}^{(b)}$ and the predictive mean $\mu^{(b)}$ in Equation (8). While the update of $(\Sigma_{oo}^{(b)})^{-1}$ can be accelerated by using the Schur complement as introduced in Section 4.2, evaluating the Fisher information matrix for each $\theta^{(j)} = (\theta_1^{(j)}, \dots, \theta_h^{(j)})$ still requires finite-difference evaluations of $\partial_{\theta_i} \mu$ and $\partial_{\theta_i} \Sigma_{oo}$, and h^2 trace terms. The final computational complexity is $O(h^2 \times N_0^2)$ since the FIM is of size $\in \mathbb{R}^{h \times h}$. Therefore the total complexity can be written as

$$O\left(J \times BM \times h^2 \times N_0^2\right),$$

which may be significantly higher than the complexity of the IMSPE or MI criteria when h is large.

5 Experiments

In this section, we evaluate and compare the performance of the MI-based criterion—together with its hybrid variant incorporating local complexity introduced in Section 3—with several classical criteria described in Section 2.3 through simulation studies. We present one numerical toy example and one real-world case study to compare all methods in terms of (i) predictive accuracy, (ii) uncertainty quantification, and (iii) design time. To this end, we employ two evaluation metrics. In the formulas below, we only discuss one-dimensional outputs, while for multi-task cases the results can be obtained by averaging across the output dimensions.

5.1 Evaluation Criteria

To assess the predictive performance of the model after experiments using the proposed design methods, we consider two evaluation criteria that measure different aspects of prediction quality. The mean squared error (MSE) evaluates the accuracy of the predictive mean, while the continuous ranked probability score (CRPS) helps account for the predictive uncertainty.

- **Mean Squared Error (MSE).** Given J posterior samples of parameters $\{\Omega^{(j)}\}_{j=1}^J$, the j -th posterior predictive mean at locations $\mathcal{X}_{\text{pred}} = \mathbf{X}^* \in \mathbb{R}^{n^* \times d}$ is obtained from (6) as $\mu_j^* = \mu_j^*(\mathbf{X}^*) \in \mathbb{R}^{n^*}$. The Bayesian predictive mean is taking the average over the J posterior samples

$$\bar{\mu}^* = \frac{1}{J} \sum_{j=1}^J \mu_j^*.$$

The true values on the predictive locations are $\mathbf{y}^* \in \mathbb{R}^{n^*}$, hence we can define the predictive mean squared error (MSE) in the Bayesian setting as

$$\text{MSE} = \|\bar{\boldsymbol{\mu}}^* - \mathbf{y}^*\|_F^2,$$

where $\|\cdot\|_F$ denotes the Frobenius norm.

- **Continuous Ranked Probability Score (CRPS).** The CRPS (Gneiting and Raftery, 2007) evaluates the quality of the full posterior predictive distribution, thus it takes account of predictive uncertainty. If we have S predictive samples

$$\mathbf{y}_1^*, \dots, \mathbf{y}_S^* \sim p(\mathbf{y}^* | \mathbf{X}^*, \mathbf{y}),$$

where each \mathbf{y}_s^* is obtained by first drawing $\boldsymbol{\Omega}^{(j)} \sim p(\boldsymbol{\Omega} | \mathbf{y})$ and then sampling $\mathbf{y}_s^* \sim p(\mathbf{y}^* | \mathbf{X}^*, \mathbf{y}, \boldsymbol{\Omega}^{(j)})$, the CRPS over the prediction set $\mathcal{X}_{\text{pred}}$ is estimated by

$$\text{CRPS} = \frac{1}{S} \sum_{s=1}^S \|\mathbf{y}_s^* - \mathbf{y}^*\|_1 - \frac{1}{2S^2} \sum_{s=1}^S \sum_{s'=1}^S \|\mathbf{y}_s^* - \mathbf{y}_{s'}^*\|_1,$$

where $\|\cdot\|_1$ denotes the element-wise ℓ_1 norm.

By monitoring these two metrics jointly, we gain a more comprehensive assessment of the KOH model’s prediction performance, not only the correct mean accuracy but also the uncertainty of the full predictive distribution across the entire design space.

5.2 Preliminaries

In this section, we will demonstrate the Bayesian experimental design setup and implementation details that are used in following two examples:

1. A simulated toy example with two calibration parameters and one controllable design input where the data-generating mechanism is known and can be evaluated at arbitrary inputs (Sections 5.3).
2. A real-world dataset ¹ drawn from cellular-signaling experiments, which contains six calibration parameters and one controllable design input (Sections 5.4).

In both case studies below, we employ sequential (offline) design of experiments (SDE) and adaptive (online) design of experiments (ADE), and we compare their performance via the metrics MSE and CRPS. The comparison includes all the classical design criteria from Section 2.3 and, importantly, the MI-based criterion together with its hybrid variant. In SDE, we additionally assess the design efficiency by comparing the runtime across different criteria under the same number of rounds, and we also further examine the computation strategies proposed in Section 4 to verify their effectiveness in reducing computational burden. The full BED setting and implementation details are as follows: to avoid unnecessary computation,

¹https://jeti.uni-freiburg.de/PNAS_Swameye_Data/

we fix the hyperparameters from the first stage GP ϕ_1 at their posterior mean. We fully account for uncertainty in the calibration parameters θ as well as the second-stage GP hyperparameters ϕ_2 by drawing 1,000 posterior samples (after burn-in) via MCMC once convergence has been reached. In particular, to compute the MI-based criterion and its hybrid variant with local complexity, we draw 10,000 predictive samples for the outer layer of the nested Monte Carlo (NMC) estimator, regardless of whether the Gaussian mixture compression technique in Section 4.1 is applied. The purpose is to ensure that the parameter uncertainty and the predictive uncertainty are both well considered and that the Monte Carlo approximation is sufficiently accurate.

All experimental design methods are implemented in PyTorch (Paszke et al., 2019) and Pyro². A key advantage of PyTorch is its native support for vectorized and matrix-based tensor operations, which allows us to avoid explicit for-loops and thereby accelerate the computations. The processing device is a laptop equipped with 16 GB DDR4-3200 RAM, an 11th Gen Intel Core i7-11800H CPU @ 2.30 GHz, and a NVIDIA RTX 3070 Ti GPU.

5.3 Simulation Case Study

Let us illustrate the settings of our first numerical toy example. The formula of the physical process which generates \mathbf{y}^p is

$$y_{\text{true}}(x) = 10 \cdot f_{\text{Gamma}}(x + 2.2; \alpha = 1.8, \lambda = 2.0) \cdot \left(1 + \sin\left(\frac{2\pi x}{1.5}\right) + 0.3 \sin\left(\frac{6\pi x}{5.0}\right) \right) + \epsilon,$$

and the formula of the computer model $y^c(\cdot, \cdot)$ is

$$y_{\text{sim}}(x, t_1, t_2) = 10 \cdot f_{\text{Gamma}}(x + 2.2; t_1, t_2).$$

Thus, the discrepancy is

$$\begin{aligned} \delta(x) &= y_{\text{true}}(x) - y_{\text{sim}}(x, 1.8, 2.0) \\ &= 10 \cdot f_{\text{Gamma}}(x + 2.2; \alpha = 1.8, \lambda = 2.0) \cdot \left(\sin\left(\frac{2\pi x}{1.5}\right) + 0.3 \sin\left(\frac{6\pi x}{5.0}\right) \right), \end{aligned}$$

where $\epsilon \sim \mathcal{N}(0, 10^{-3})$, the input domain is $x \in [-2, 8]$, the first calibration parameter follows the prior $t_1 \sim \text{Uniform}(0.8, 2.6)$, the second calibration parameter follows the prior $t_2 \sim \text{Uniform}(1, 3.5)$, and the true values for the calibration parameters are $\alpha = 1.8$ and $\lambda = 2$, respectively. The original training points (5 field observations and 30 simulator data points) are generated using a Maximin Latin Hypercube Design inside the input domain. We generate 50 candidate design points $\mathcal{D}_{\text{cand}}$ on a uniform grid over the input domain, and then fix 100 prediction points $\mathcal{X}_{\text{pred}}$ also uniformly distributed across the domain, without overlapping. The computer model $y^c(\cdot, \cdot)$ employs a GP prior with zero mean and a Radial Basis Function (RBF) kernel parameterized by four hyperparameters that are given weakly informative priors. For the discrepancy term, we adopt an ‘‘RBF \times periodic’’ kernel with the first stage GP output as mean function. Moreover, the pattern of predictive means exhibits substantial spatial variability, so for the hybrid criteria we assign equal weights

²<https://docs.pyro.ai/en/stable/contrib.oed.html>

($\alpha = 0.5$) to the predictive uncertainty and local model complexity in both Equation (14) and Equation (15).

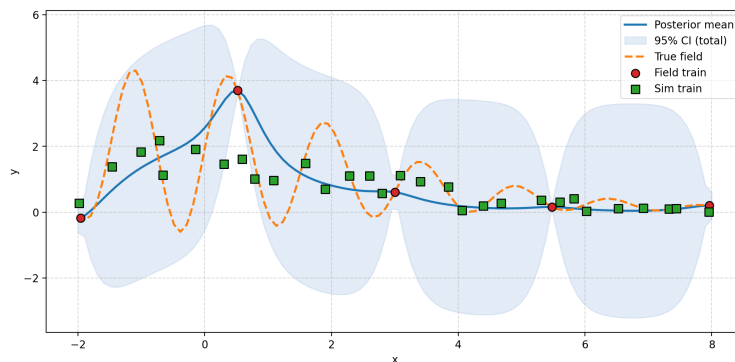
We implement the two design strategies SDE and ADE described in Section 2.2 for a total of 10 rounds. Firstly, to provide a visual illustration, Figure 2 shows the model regression before and after 10 rounds of ADE using the Mutual Information + Local Complexity Maximization (MI+CX) criterion. From Figure 2, we observe that the regression improves substantially, reflected both in the increased accuracy of the predictive mean and in the reduction of predictive uncertainty. One of our primary interests here lies in comparing the performance of the different design criteria under both SDE and ADE. Figure 3 displays heatmaps of the average performance for the six criteria evaluated across 10 design rounds in this toy example, shown separately for evaluation metrics (a) MSE and (b) CRPS. It is obvious that the MI+CX criterion performs the best under both SDE and ADE, achieving the lowest average MSE and CRPS among all methods. Moreover, when the IMSPE minimization criterion is augmented with local complexity (IMSPE+CX), it achieves an improvement compared to plain IMSPE. Intuitively, ADE consistently outperforms SDE across all criteria except Maximin distance, and the improvement is substantial if we revisit Figure 3. This indicates that updating the posterior after each new observation is typically beneficial, which enables the criteria to choose experimental locations more effectively. Additionally, Figure 4 compares the performance of each criterion at the final round for (a) MSE and (b) CRPS. The pattern is consistent with the 10-round average performance shown in Figure 3: the MI+CX criterion continues to achieve the best performance, followed by D-optimality and the MI-based criterion, under both SDE and ADE.

In Section 3.2, we introduced a hybrid design criterion that incorporates a local model complexity adjustment into mutual information gain. From these plots, it is evident that the hybrid variant consistently outperforms the pure MI-based criterion, regardless of whether the strategy is SDE or ADE. This provides clear empirical support for the effectiveness of incorporating local model complexity into the MI-based design criterion.

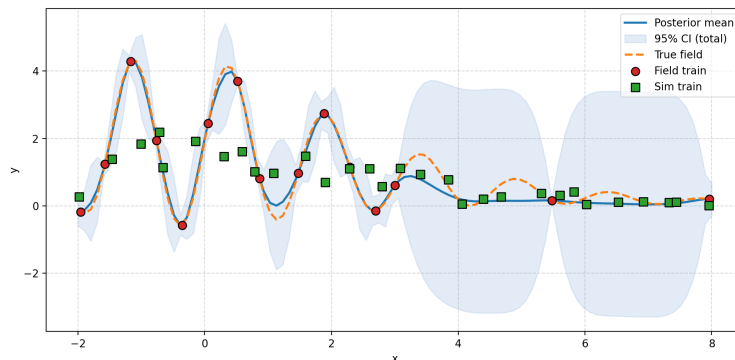
We also examine the theoretical property established in Theorem 1. As shown in Figure 3, the number of initial physical observations is small, and the underlying model is highly uncertain. This causes learning difficulties in the early design stages. Therefore, we intentionally apply both criteria for an additional 10 rounds after the first 10 rounds of design under both SDE and ADE. A total of 20 rounds are conducted, and the results are reported in Figure 5. By checking the figure, we observe that the gap in MSE and CRPS between the two criteria gradually decreases as the design rounds proceed. By around the twentieth round, the predictive improvement offered by the two criteria becomes almost equivalent. This is empirically consistent with the theoretical result we established—namely, the local asymptotic relationship between MI and IMSPE in Theorem 1.

Another primary objective is to assess the computational efficiency of the design criteria in the SDE setting by comparing their design times over 10 rounds. Table 1 summarizes the results. We observe that by employing the Gaussian Mixture Compression strategy, the computation time of the MI-based criterion is substantially reduced, while still maintaining excellent performance. Note that the heatmaps in Figure 3 shown are using the results from the compression strategy. We also observe that, relative to MI and MI+CX, the IMSPE minimization criterion is extremely fast, while the D-optimality criterion is more computationally expensive. Therefore, if we jointly consider both design time and predic-

tive performance from Figure 3 and Figure 4, we find that the performance of IMSPE and D-optimality is not necessarily poor. In fact, the D-optimality criterion performs reasonably well although it is originally aimed to improve the estimation of model parameters. Finally, note that in SDE we use the precomputation and Schur complement update technique (Section 4.2) by default, so no performance comparison with respect to this computation strategy is included. In our experience, however, this strategy also yields substantial computational savings.



(a) Original regression for toy example

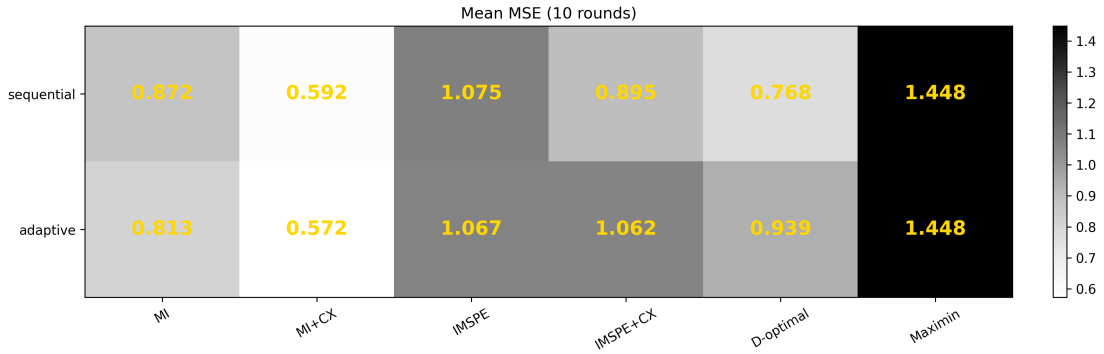


(b) Regression after 10 rounds for toy example using MI+CX criterion under ADE

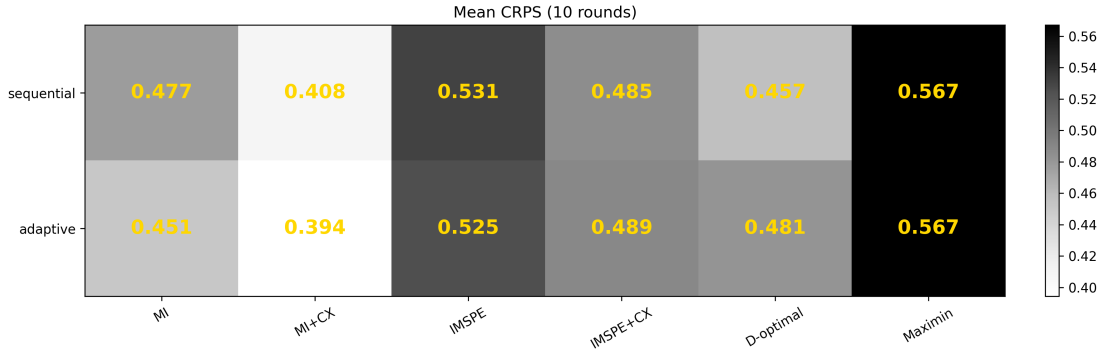
Figure 2: Simulation case: comparison of (a) the original model regression and (b) after design model regression.

5.4 Real-World Data Analysis

We now move to our second example, in which we perform sequential Bayesian experimental design (BED) using a real-world biochemical dataset. Swameye et al. (2003) introduced a family of parameterized ordinary differential equation (ODE) models to describe the dynamics of the JAK–STAT5 signaling pathway. This pathway is characterized by the rapid shuttling of STAT5 between the nucleus and cytoplasm in response to upstream activation, accompanied by a series of tightly regulated biochemical reactions. Because all intermediate quantities in the pathway vary rapidly, real-time active learning at the experimental site is



(a) Heatmap of the mean MSE over 10 rounds for design criteria under SDE and ADE for the toy model

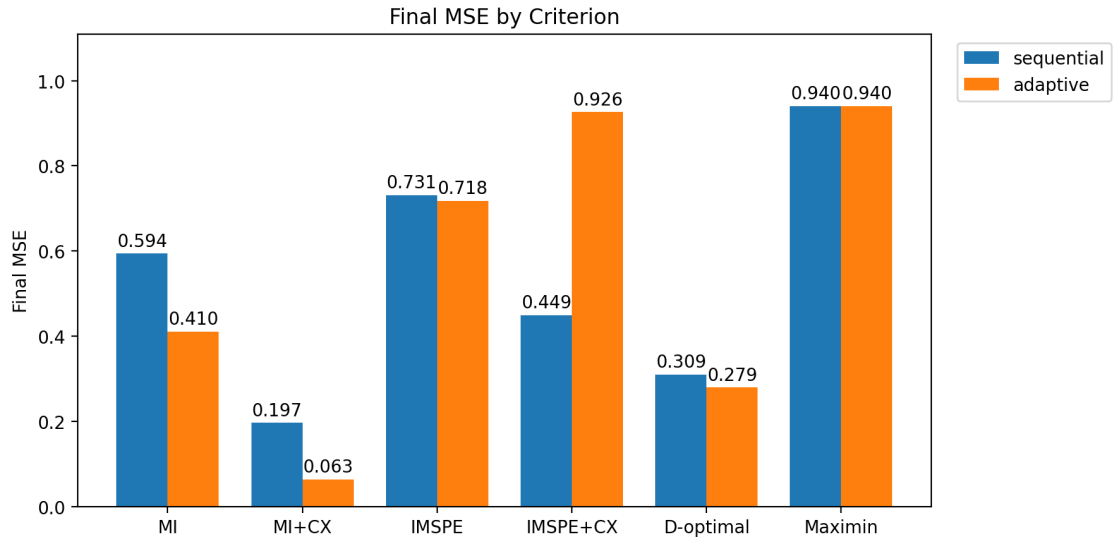


(b) Heatmap of the mean CRPS over 10 rounds for design criteria under SDE and ADE for the toy model

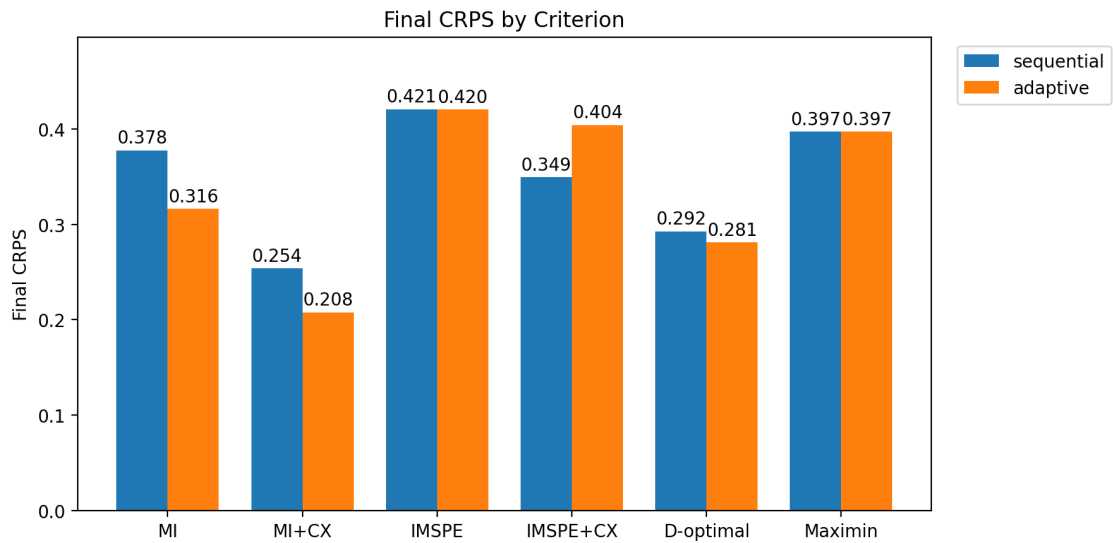
Figure 3: Simulation case: comparison of average (a) MSE and (b) CRPS for each criterion across 10 design rounds.

Table 1: Computation time comparison for different design criteria over 10 sequential (offline) design (SDE) rounds of the toy model.

Method	Time [s]	Time [min]
Mutual Information Gain (Gaussian Mixture Compression)	142.0512	2.368
Mutual Information Gain + Complexity (Gaussian Mixture Compression)	143.1869	2.386
Mutual Information Gain (Naive NMC)	901.4012	15.023
Mutual Information Gain + Complexity (Naive NMC)	902.8288	15.047
Integrated Mean Square Prediction Error	10.0309	0.167
Integrated Mean Square Prediction Error + Complexity	10.7311	0.179
D-optimality	295.0461	4.917
Maximin Distance	0.0160	0.000

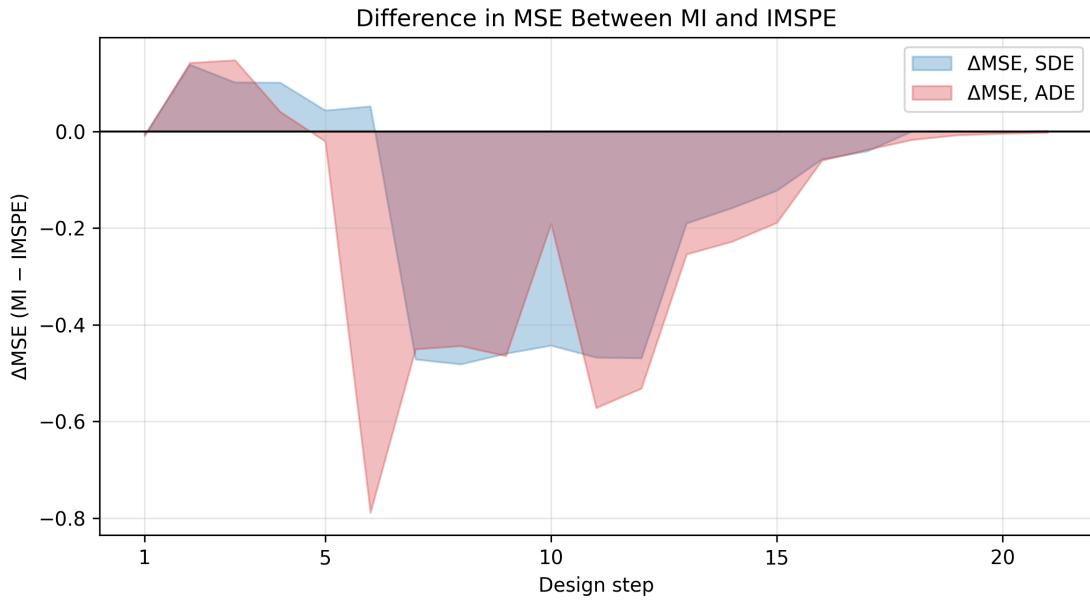


(a) MSE of final round for design criteria under SDE and ADE for the toy model

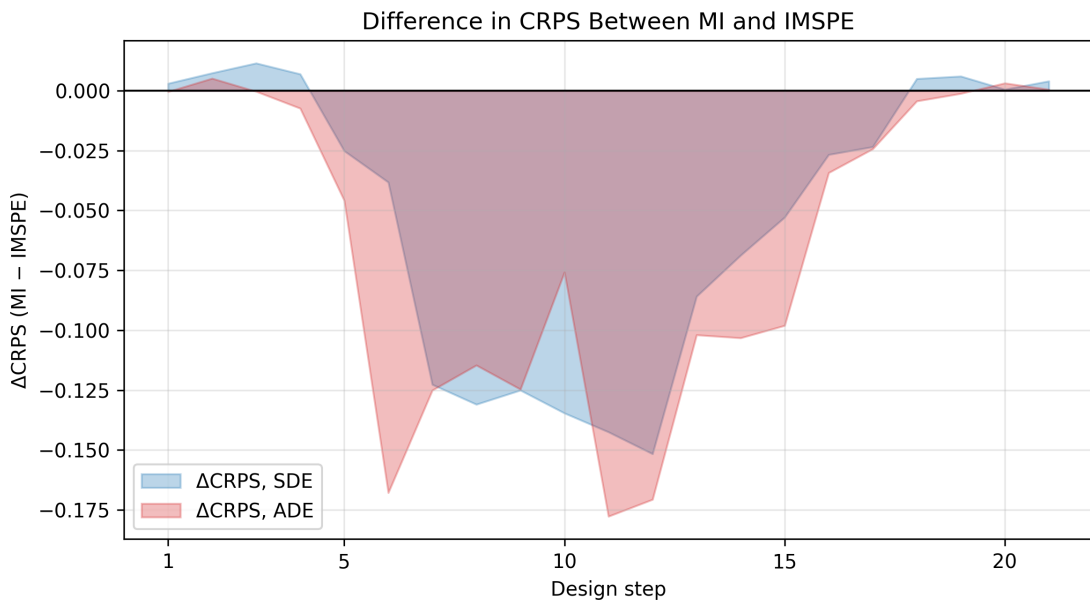


(b) CRPS of final round for design criteria under SDE and ADE for the toy model

Figure 4: Simulation case: comparison of final-round (a) MSE and (b) CRPS for each criterion.



(a) The MSE difference of the MI-based criterion and IMSPE minimization over 20 rounds under SDE and ADE for the toy model



(b) The CRPS difference of the MI-based criterion and IMSPE minimization over 20 rounds under SDE and ADE for the toy model

Figure 5: Simulation case: comparison of (a) ΔMSE and (b) ΔCRPS for the MI-based criterion and IMSPE minimization over 20 rounds.

infeasible. In contrast, collecting measurements of STAT5 population concentrations at a limited number of time points is much more practical.

In addition, [Swameye et al. \(2003\)](#) collected experimental measurements from a time-course study and a β -Galactosidase Assay. Through the observation data and mechanistic modeling, the researchers can analyze the quantitative behavior of STAT5 populations as well as the parameter sensitivities. Following [Swameye et al. \(2003\)](#) and [Kirk and Stumpf \(2009\)](#), we therefore can adopt an ODE framework to describe this dynamic cycle/pathway:

$$\begin{aligned}\frac{dv_1}{dt} &= -p_1 v_1 D + 2p_4 v_4, \\ \frac{dv_2}{dt} &= p_1 v_1 D - v_2^2, \\ \frac{dv_3}{dt} &= -p_3 v_3 + 0.5 v_2^2, \\ \frac{dv_4}{dt} &= p_3 v_3 - p_4 v_4.\end{aligned}$$

$$\begin{cases} x_1 = p_5(v_1 + v_2 + 2v_3), \\ x_2 = p_6(v_2 + 2v_3). \end{cases}$$

Here, D denotes the cytokine input that activates the biochemical reactions. It is initially controlled by the experimenter but varies over time. The state variables v_1, v_2 and v_3 represent the concentrations of unphosphorylated cytoplasmic STAT5 in different phases of the signaling cycle, while v_4 is the nuclear STAT5 concentration. The initial concentration $v_1(t=0)$ is treated as an unknown calibration parameter, while the other initial concentrations are assumed at zero: $v_2(t=0) = v_3(t=0) = v_4(t=0) = 0$. The reaction rates p_1, p_3, p_4 and the scaling factors p_5, p_6 are also treated as calibration parameters. Since the individual state concentrations v_1, \dots, v_4 cannot be directly observed, the only measurable outputs are $x_1 = \text{“total cytoplasmic STAT5”}$ and $x_2 = \text{“phosphorylated cytoplasmic STAT5”}$. Thus, the full calibration vector is $\boldsymbol{\theta} = p_1, p_3, p_4, p_5, p_6, v_1(t=0)$, and the simulator output is $\mathbf{y}^s = (x_1, x_2)$.

We consider the time window $t \in [0, 60]$ minutes. Following [Kirk and Stumpf \(2009\)](#), we use their reported ‘optimal’ calibration parameter values as reference points: $v_1(t=0) = 0.996$, $p_1 = 2.43$, $p_3 = 0.256$, $p_4 = 0.303$, $p_5 = 1.27$, and $p_6 = 0.944$. Based on these values, we specify reasonably wide prior ranges that remain realistic for the parameters: $v_1(t=0) \sim \text{Uniform}(0.8, 1.1)$, $p_1 \sim \text{Uniform}(2.1, 2.8)$, $p_3 \sim \text{Uniform}(0.1, 0.4)$, $p_4 \sim \text{Uniform}(0.1, 0.4)$, $p_5 \sim \text{Uniform}(1, 1.5)$ and $p_6 \sim \text{Uniform}(0.7, 1.4)$. The dataset contains 19 field observations (D, x_1, x_2) at discrete time points. We apply a maximin Latin hypercube design to select 4 of these as the initial training set. The simulator/computer model is run at 60 equally spaced time inputs over the 0–60 min interval through a Runge-Kutta routine. The candidate set $\mathcal{D}_{\text{cand}}$ consists of 60 equally spaced time points over the interval $[1, 60]$. This grid is shifted relative to the simulator training inputs, which are defined on $[0, 60]$, so that the two sets of time points do not overlap. The future prediction set $\mathcal{X}_{\text{pred}}$ contains 100 uniformly spaced time points over $[0, 60]$. Throughout both stages of the KOH model, we use RBF kernels for the GPs. Because the outputs x_1 and x_2 are correlated, we employ a multi-output GP with a

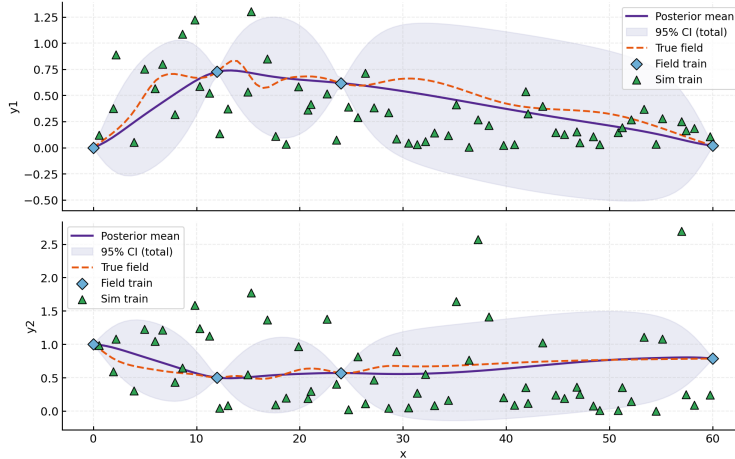
Kronecker-structured kernel that combines the RBF input kernel with an output covariance kernel to capture cross-output dependence. One practical problem is that the 19 physical observations are too sparse to evaluate predictive performance after design. We therefore interpolate the full set of observations to construct a denser pseudo “ground truth” series. From exploratory model fitting, we find that the local complexity does not vary noticeably across the time range, so we set $\alpha = 0.3$ in both Equation (14) and Equation (15).

We still conduct 10 sequential rounds of both SDE and ADE to evaluate how each design criterion improves the predictive performance of the KOH model. Figure 6 first compares the regression fitted by the original physical observations to the regression after applying the MI+CX criterion for 10 rounds of ADE. Consistent with the findings in Section 5.3, under ADE the MI+CX criterion continues to outperform all the other criteria. For the layout of Figure 6, each subplot contains two fitted curves along with their associated confidence intervals, which correspond to the two correlated outputs x_1 and x_2 . The heatmaps in Figure 7 demonstrate the average predictive performance of the six design criteria after 10 rounds of SED and ADE, with panel (a) displaying the mean MSE and panel (b) the mean CRPS. In the JAK–STAT5 example, the differences among criteria are less pronounced than in the toy example. The underlying reason is that the true data-generating curve is not highly complex, and the additional 10 physical observations can provide sufficient information for accurate learning. From Figure 7(a), we observe that MI+CX criterion still yields the best overall predictive accuracy under both SDE and ADE, achieving the lowest MSE. It is worth to note that the D-optimality criterion performs almost as well in comparison, ranking second only to MI+CX, since well-calibrated parameters naturally lead to strong predictive performance. This advantage becomes even more evident in 7(b), where the D-optimality criterion achieves the lowest CRPS under ADE, indicating the largest reduction in predictive uncertainty. The MI-based criterion also performs relatively well. Although MI+CX is not the best in terms of CRPS, MI+CX remains the most robust criterion in this case study if MSE and CRPS are evaluated jointly. Figure 8 further confirms this point by checking the final-round performance. In terms of MSE, MI+CX clearly outperforms all other criteria by a noticeable margin, followed by D-optimality and MI-based design. For CRPS, under ADE all criteria except maximin distance yield nearly indistinguishable results, but under SDE, MI+CX still shows a slight advantage.

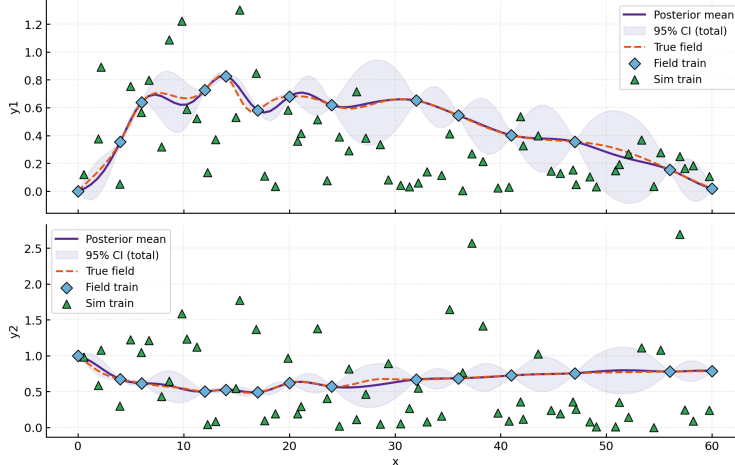
Let us also evaluate the design time in this example. Over 10 rounds of SDE, the computational efficiency of the MI-based criteria again exhibits a substantial difference depending on whether the Gaussian Mixture Compression strategy is adopted or not. The IMSPE and IMSPE+CX criteria are still very fast, although their predictive performance is relatively poor, as shown in Figure 7 and Figure 8. In the JAK–STAT5 example, the D-optimality criterion becomes the most computationally expensive criterion since the JAK–STAT5 signaling pathway system involves six calibration parameters and two responses, amplifying the computational burden substantially.

6 Conclusion and Discussion

Many studies have shown that the Kennedy & O’Hagan (KOH) model can achieve high fidelity to the underlying physical process. In some cases of model misspecification, where



(a) Original regression for the JAK-STAT5 example

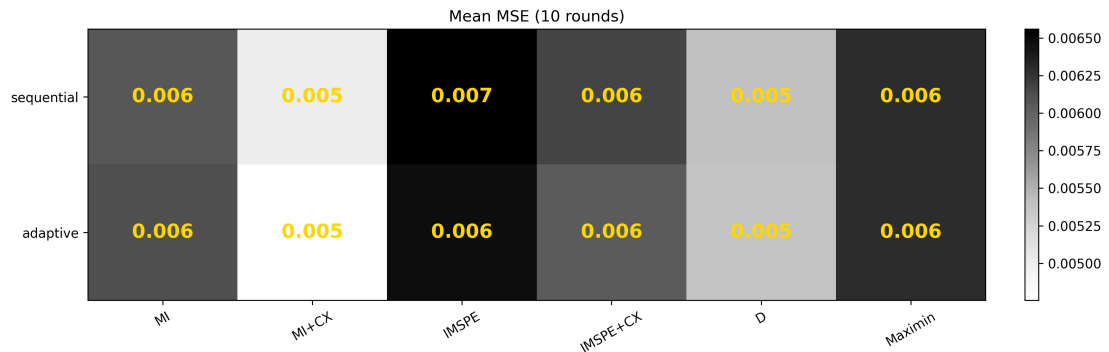


(b) Regression after 10 rounds for the JAK-STAT5 example using MI+CX criterion under ADE

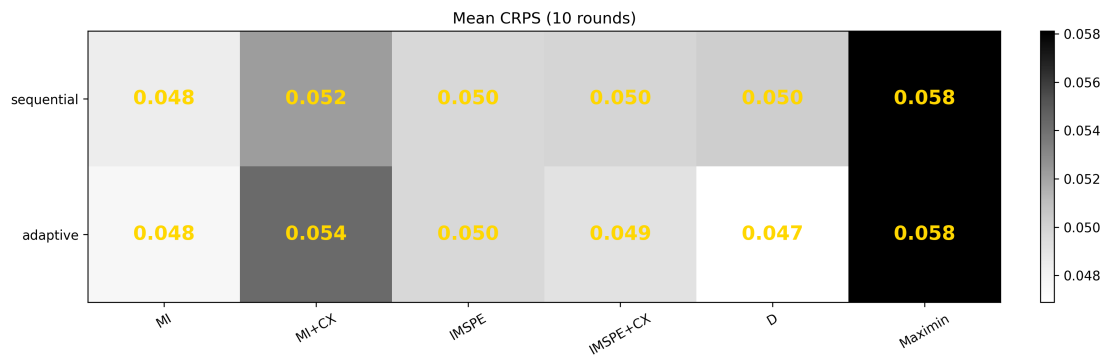
Figure 6: JAK-STAT5 example: comparison of (a) the original model regression and (b) after design model regression.

Table 2: Computation time comparison for different design criteria over 10 sequential (offline) design (SDE) rounds of the JAK-STAT5 example.

Method	Time [s]	Time [min]
Mutual Information Gain (Gaussian Mixture Compression)	435.2585	7.254
Mutual Information Gain + Complexity (Gaussian Mixture Compression)	438.8006	7.313
Mutual Information Gain (Naive NMC)	2761.9797	46.033
Mutual Information Gain + Complexity (Naive NMC)	2784.4565	46.408
Integrated Mean Square Prediction Error	67.1493	1.119
Integrated Mean Square Prediction Error + Complexity	68.9452	1.149
D-optimality	2831.5098	47.192
Maximin Distance	0.0223	0.000

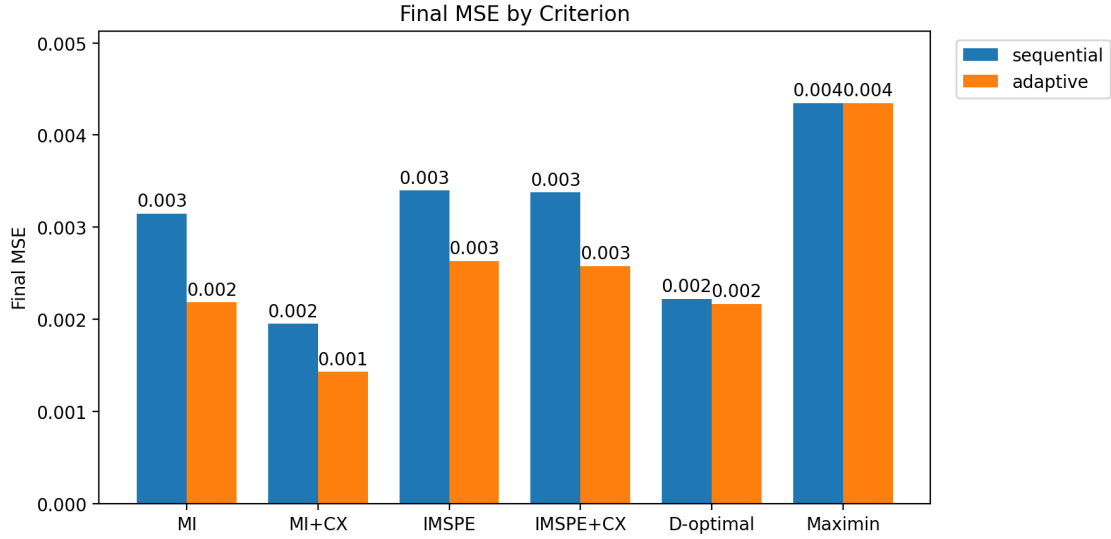


(a) Heatmap of the mean MSE over 10 rounds for design criteria under SDE and ADE for the JAK-STAT5 example

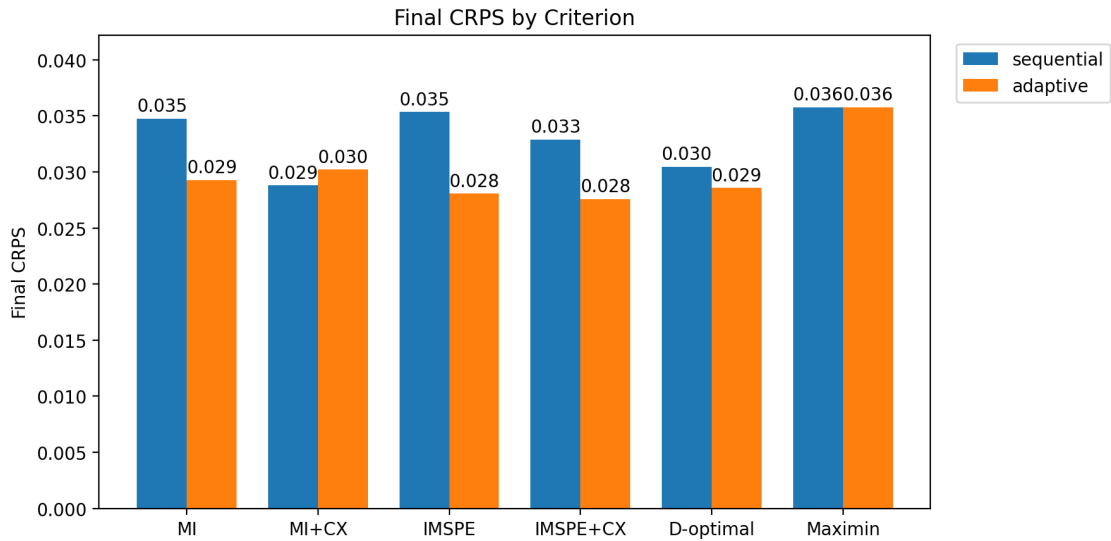


(b) Heatmap of the mean CRPS over 10 rounds for design criteria under SDE and ADE for the JAK-STAT5 example

Figure 7: JAK-STAT5 example: comparison of average (a) MSE and (b) CRPS for each criterion across 10 design rounds.



(a) MSE of final round for design criteria under SDE and ADE for the JAK-STAT5 example



(b) CRPS of final round for design criteria under SDE and ADE for the JAK-STAT5 example

Figure 8: JAK-STAT5 example: comparison of final-round (a) MSE and (b) CRPS for each criterion.

the computer model’s structural error remains regardless of how well its parameters are calibrated, the physical observations play a crucial role as they correct the discrepancy between the computer model and reality. From this perspective, the entire KOH model is viewed as an augmented “simulator” and the subsequent physical experiments become essential for improving the model capacity. In this work, we address a previously under-explored gap of the KOH framework: the sequential Bayesian design of physical experiments with the explicit goal of improving the KOH model’s predictive performance, while considering all sources of uncertainty.

A well-known challenge in Bayesian experimental design (BED) is the heavy computation burden since each design round typically requires updating the parameter posterior as well as the marginal predictive distribution. A naive implementation often relies on the nested Monte Carlo (NMC) estimator, whose computational cost increases rapidly with the number of samples. Although many modern approaches alleviate this expense by introducing variational lower bounds or amortized approximations (Foster et al., 2019; Kleingesse and Gutmann, 2021; Poole et al., 2019), our goal in this work is to obtain sufficiently accurate evaluations of design criteria across a bunch of closely competing candidate inputs. Therefore, the naive NMC estimator remains an attractive choice because it enjoys almost-sure convergence as demonstrated in Section 3.3. Also, it is important to note that the NMC estimator is notably robust in high-dimensional predictive spaces and when the distributions are multi-modal, heavy-tailed, or exhibit complex dependence structures. In adaptive (online) design of experiments (ADE), amortized policy-based approaches, most notably Foster et al. (2021), significantly reduce the per-round computational cost by learning a reusable design policy. However, in many practical scenarios true ADE is infeasible as conducting physical experiments in real time can be costly or technically difficult. Meanwhile, the cost of amortization, which is incurred mostly due to training a neural network, is also expensive and only worthwhile when a large number of repeated design tasks are required, whereas in many practical scenarios this is not the case. The importance of sequential (offline) design of experiments (SDE) is underrated in many situations. It enables sequential design decisions without conducting actual experiments during the design stage, making it especially suitable when field data acquisition is slow or difficult.

Because the SDE used in our work is inherently greedy, it may be prone to getting trapped in local optima rather than achieving a global optimal design. To mitigate this limitation, our key innovation is the introduction of composite design criteria that combine uncertainty reduction objectives (MI-based or IMSPE minimization) with measures of local complexity (gradient magnitude and discrete gradient variation). The experimental results in Section 5 demonstrate that the proposed Mutual Information + Local Complexity Maximization (MI+CX) criterion consistently outperforms all other alternatives, especially where the predictive surface exhibits sharp local variations.

We further contribute a set of computational strategies to reduce the overall computational complexity of the different criteria considered in this work under the choice of using the NMC estimator. The Gaussian Mixture Compression technique introduced in Section 4.1 is applied to the MI-based criterion, IMSPE minimization, and their hybrid variants in BED. It effectively reduces the number of components in the Gaussian mixture representation of the predictive distribution. The second strategy of using precomputations and Schur complement updates can be applied to nearly all criteria that require covariance matrix operations.

This strategy is particularly well-suited to the SDE setting since the parameter posterior remains fixed across rounds.

In Section 3.3, we establish the theoretical relationship between the MI-based criterion and the IMSPE minimization criterion. The IMSPE minimization approach has been frequently used in design problems aimed at improving predictive performance. However, its reliance solely on the trace of the predictive covariance matrix inevitably leads to information loss to some extent, since it does not account for the full covariance structure in the way the MI-based criterion does. Compared to the IMSPE minimization criterion, the MI-based criterion is a more comprehensive and robust measure, especially during the early stages of experiments when the observations are sparse. As shown in Theorem 1, the MI-based criterion converges to a fixed scale of the IMSPE minimization criterion once the design has progressed sufficiently far that the covariance matrix changes only marginally. In this asymptotic regime, the two utilities are equivalent up to a constant factor.

The proposed hybrid criterion MI+CX is both effective and computationally efficient under both ADE and SDE. Some restrictions still remain that future work may seek to address. First, the ADE and SDE strategies applied in this paper are entirely myopic. These frameworks could be extended to batch or fully non-myopic design strategies. For example, multi-step lookahead schemes or approaches based on reinforcement learning can explicitly optimize far-sighted utilities. Second, our empirical studies in this paper focus exclusively on one-dimensional controllable design inputs. Extending the methodology to multivariate or high-dimensional design spaces is essential for many real applications. Marmin and Filippone (2022) has demonstrated that deep Gaussian processes combined with random feature expansions can effectively handle high-dimensional inputs and complex non-stationary structures within the KOH framework. Integrating these advances with our proposed design criteria can further enhance the performance and robustness of sequential Bayesian experimental design in challenging settings.

Acknowledgments

The authors were supported by the Linz Institute of Technology’s grant LIFT_C-2022-1-123 funded by the State of Upper Austria and Austria’s Federal Ministry of Education, Science and Research.

Appendix A Proof of Theoretical Properties

Theorem 1 (Local asymptotic relationship between MI and IMSPE). *Assume that, (i) conditional on Ω , $(\mathbf{y}^*, \mathbf{y}_{(b)}^{\text{new}})$ is jointly Gaussian, (ii) $\Sigma_{(b-1)}^*$ is symmetric positive definite with eigenvalues $0 < \lambda_{\min} \leq \lambda_{\max} < \infty$. Define the covariance reduction and IMSPE reduction at round b as*

$$\Delta \Sigma^*(\boldsymbol{\xi}_{(b)}) := \Sigma_{(b-1)}^* - \Sigma_{(b)}^* \succeq \mathbf{0}, \quad \Delta \text{IMSPE}(\boldsymbol{\xi}_{(b)} \mid \Omega) := \frac{1}{n^*} \text{tr}(\Delta \Sigma^*(\boldsymbol{\xi}_{(b)})).$$

As the sequential design rounds proceed, the following small-update regime holds:

$$\|(\Sigma_{(b-1)}^*)^{-1/2} \Delta \Sigma^*(\boldsymbol{\xi}_{(b)}) (\Sigma_{(b-1)}^*)^{-1/2}\|_2 \rightarrow 0.$$

Then there exists a finite constant C_{b-1} , depending on $\Sigma_{(b-1)}^*$, such that

$$\frac{U(\boldsymbol{\xi}_{(b)} \mid \boldsymbol{\Omega})}{\Delta \text{IMSPE}(\boldsymbol{\xi}_{(b)} \mid \boldsymbol{\Omega})} \longrightarrow C_{b-1} \quad \text{as} \quad \Delta \Sigma^*(\boldsymbol{\xi}_{(b)}) \rightarrow \mathbf{0},$$

and this constant is bounded in terms of the eigenvalues of $\Sigma_{(b-1)}^*$:

$$\frac{n^*}{2 \lambda_{\max}(\Sigma_{(b-1)}^*)} \leq C_{b-1} \leq \frac{n^*}{2 \lambda_{\min}(\Sigma_{(b-1)}^*)}.$$

Proof. Throughout the proof we condition on $\boldsymbol{\Omega}$. For brevity, write

$$\Sigma_0 := \Sigma_{(b-1)}^*, \quad \Sigma_1 := \Sigma_{(b)}^*, \quad \Delta \Sigma := \Delta \Sigma^*(\boldsymbol{\xi}_{(b)}) = \Sigma_0 - \Sigma_1 \succeq \mathbf{0}.$$

By definition,

$$\Delta \text{IMSPE}(\boldsymbol{\xi}_{(b)} \mid \boldsymbol{\Omega}) = \frac{1}{n^*} \text{tr}(\Delta \Sigma).$$

According to Assumption (i), the mutual information formula has the closed-form expression

$$U(\boldsymbol{\xi}_{(b)} \mid \boldsymbol{\Omega}) = I(\mathbf{y}^*; \mathbf{y}_{(b)}^{\text{new}} \mid \boldsymbol{\Omega}, \mathcal{D}_{\text{sel}}^b) = \frac{1}{2} \left(\log \det \Sigma_0 - \log \det \Sigma_1 \right).$$

According to Assumption (ii), Σ_0 is symmetric positive definite, so we can rewrite Σ_1 and the standardized covariance reduction \mathbf{B} as

$$\Sigma_1 = \Sigma_0 - \Delta \Sigma = \Sigma_0^{1/2} (\mathbf{I}_{n^*} - \mathbf{B}) \Sigma_0^{1/2}, \quad \mathbf{B} := \Sigma_0^{-1/2} \Delta \Sigma \Sigma_0^{-1/2} \succeq \mathbf{0}.$$

Then

$$U(\boldsymbol{\xi}_{(b)} \mid \boldsymbol{\Omega}) = -\frac{1}{2} \log \det(\mathbf{I}_{n^*} - \mathbf{B}).$$

Let $\tau_1, \dots, \tau_{n^*}$ be the eigenvalues of \mathbf{B} . Since $\mathbf{B} \succeq \mathbf{0}$, $\tau_i \geq 0$ and

$$\log \det(\mathbf{I}_{n^*} - \mathbf{B}) = \sum_{i=1}^{n^*} \log(1 - \tau_i),$$

so

$$U(\boldsymbol{\xi}_{(b)} \mid \boldsymbol{\Omega}) = -\frac{1}{2} \sum_{i=1}^{n^*} \log(1 - \tau_i).$$

Under the small-update regime as the design rounds progress, the operator norm of \mathbf{B}

$$\|\mathbf{B}\|_2 = \|(\Sigma_{(b-1)}^*)^{-1/2} \Delta \Sigma^*(\boldsymbol{\xi}_{(b)}) (\Sigma_{(b-1)}^*)^{-1/2}\|_2 \longrightarrow 0,$$

thus $\max_i \tau_i \rightarrow 0$.

Taking the second-order Taylor expansion of $U(\boldsymbol{\xi}_{(b)} \mid \boldsymbol{\Omega})$, we can have, for all sufficiently large b ,

$$U(\boldsymbol{\xi}_{(b)} \mid \boldsymbol{\Omega}) = \frac{1}{2} \sum_{i=1}^{n^*} \tau_i + R_b,$$

and each Taylor remainder is bounded by τ_i^2 . Since $\|\mathbf{B}\|_2 \rightarrow 0$, for any $\varepsilon > 0$ there exists b_0 such that for all $b \geq b_0$, $\|\mathbf{B}\|_2 < \varepsilon$. For convenience, we here choose $\varepsilon = 1/2$. Hence for all sufficiently large b , we $\|\mathbf{B}\|_2 < 1/2$, and therefore $0 \leq \tau_i < 1/2$ for all i . For each i , define

$$r(\tau_i) := -\log(1 - \tau_i) - \tau_i.$$

Since $0 \leq \tau_i < 1/2$, the Taylor expansion of $-\log(1 - \tau_i)$ at 0 is valid and gives

$$-\log(1 - \tau_i) = \tau_i + \sum_{k=2}^{\infty} \frac{\tau_i^k}{k},$$

so that

$$r(\tau_i) = \sum_{k=2}^{\infty} \frac{\tau_i^k}{k}, \quad R_b = \frac{1}{2} \sum_{i=1}^{n^*} r(\tau_i).$$

Moreover, for each i ,

$$0 \leq r(\tau_i) = \sum_{k=2}^{\infty} \frac{\tau_i^k}{k} \leq \frac{1}{2} \sum_{k=2}^{\infty} \tau_i^k = \frac{1}{2} \cdot \frac{\tau_i^2}{1 - \tau_i} \leq \tau_i^2,$$

where we used $1/k \leq 1/2$ for all $k \geq 2$ and $1 - \tau_i \geq 1/2$. Therefore,

$$|R_b| = \frac{1}{2} \sum_{i=1}^{n^*} r(\tau_i) \leq \frac{1}{2} \sum_{i=1}^{n^*} \tau_i^2.$$

Using the cyclic invariance of the trace

$$\sum_{i=1}^{n^*} \tau_i = \text{tr}(\mathbf{B}) = \text{tr}(\boldsymbol{\Sigma}_0^{-1} \Delta \boldsymbol{\Sigma}), \quad \sum_{i=1}^{n^*} \tau_i^2 = \|\mathbf{B}\|_F^2,$$

we obtain

$$U(\boldsymbol{\xi}_{(b)} | \boldsymbol{\Omega}) = \frac{1}{2} \text{tr}(\boldsymbol{\Sigma}_0^{-1} \Delta \boldsymbol{\Sigma}) + R_b, \quad |R_b| \leq \frac{1}{2} \|\mathbf{B}\|_F^2. \quad (17)$$

We divide $U(\boldsymbol{\xi}_{(b)} | \boldsymbol{\Omega})$ by $\Delta \text{IMSPE}(\boldsymbol{\xi}_{(b)} | \boldsymbol{\Omega})$, then obtain

$$\frac{U(\boldsymbol{\xi}_{(b)} | \boldsymbol{\Omega})}{\Delta \text{IMSPE}(\boldsymbol{\xi}_{(b)} | \boldsymbol{\Omega})} = \frac{n^*}{2} \frac{\text{tr}(\boldsymbol{\Sigma}_0^{-1} \Delta \boldsymbol{\Sigma})}{\text{tr}(\Delta \boldsymbol{\Sigma})} + \frac{n^*}{\text{tr}(\Delta \boldsymbol{\Sigma})} R_b. \quad (18)$$

By the standard trace inequality for symmetric $\boldsymbol{\Sigma}_0^{-1} \succ \mathbf{0}$ and $\Delta \boldsymbol{\Sigma} \succeq \mathbf{0}$,

$$\lambda_{\min}(\boldsymbol{\Sigma}_0^{-1}) \text{tr}(\Delta \boldsymbol{\Sigma}) \leq \text{tr}(\boldsymbol{\Sigma}_0^{-1} \Delta \boldsymbol{\Sigma}) \leq \lambda_{\max}(\boldsymbol{\Sigma}_0^{-1}) \text{tr}(\Delta \boldsymbol{\Sigma}),$$

and since $\lambda_{\min}(\boldsymbol{\Sigma}_0^{-1}) = 1/\lambda_{\max}$, $\lambda_{\max}(\boldsymbol{\Sigma}_0^{-1}) = 1/\lambda_{\min}$, we thus obtain the interval of the first term in (18):

$$\frac{n^*}{2 \lambda_{\max}} \leq \frac{n^*}{2} \frac{\text{tr}(\boldsymbol{\Sigma}_0^{-1} \Delta \boldsymbol{\Sigma})}{\text{tr}(\Delta \boldsymbol{\Sigma})} \leq \frac{n^*}{2 \lambda_{\min}}. \quad (19)$$

For the remainder term R_b , we use the cyclic invariance of the trace again, then

$$\Delta\Sigma = \Sigma_0^{1/2}\mathbf{B}\Sigma_0^{1/2}, \quad \text{so} \quad \text{tr}(\Delta\Sigma) = \text{tr}(\mathbf{B}\Sigma_0) = \sum_{i=1}^{n^*} \tau_i \mathbf{v}_i^\top \Sigma_0 \mathbf{v}_i \geq \lambda_{\min} \sum_{i=1}^{n^*} \tau_i,$$

where $\{\mathbf{v}_i\}$ is an eigenbasis of \mathbf{B} . Moreover, $\sum_i \tau_i^2 \leq (\max_i \tau_i) \sum_i \tau_i = \|\mathbf{B}\|_2 \sum_i \tau_i$, so

$$\frac{|R_b|}{\text{tr}(\Delta\Sigma)} \leq \frac{\frac{1}{2} \sum_i \tau_i^2}{\lambda_{\min} \sum_i \tau_i} \leq \frac{1}{2\lambda_{\min}} \|\mathbf{B}\|_2 \rightarrow 0 \quad \text{as} \quad \Delta\Sigma^*(\boldsymbol{\xi}_{(b)}) \rightarrow \mathbf{0}.$$

Together with (18) and (19)

$$\frac{U(\boldsymbol{\xi}_{(b)} \mid \boldsymbol{\Omega})}{\Delta\text{IMSPE}(\boldsymbol{\xi}_{(b)} \mid \boldsymbol{\Omega})} = \frac{n^* \text{tr}(\Sigma_0^{-1} \Delta\Sigma)}{2 \text{tr}(\Delta\Sigma)} + o(1).$$

Hence any limit

$$C_{b-1} := \lim_{\Delta\Sigma^*(\boldsymbol{\xi}_{(b)}) \rightarrow \mathbf{0}} \frac{U(\boldsymbol{\xi}_{(b)} \mid \boldsymbol{\Omega})}{\Delta\text{IMSPE}(\boldsymbol{\xi}_{(b)} \mid \boldsymbol{\Omega})}$$

is finite and C_{b-1} is between $\frac{n^*}{2\lambda_{\max}}$ and $\frac{n^*}{2\lambda_{\min}}$

$$\frac{n^*}{2\lambda_{\max}(\Sigma_{(b-1)}^*)} \leq C_{b-1} \leq \frac{n^*}{2\lambda_{\min}(\Sigma_{(b-1)}^*)}.$$

□

Lemma 1 (Smoothness and bounded derivatives of the outer-layer function). *Let the outer-layer function of the proposed NMC estimator be the log function $f : \mathbb{R}_+ \rightarrow \mathbb{R}$, $x \mapsto \log(x)$. Let the argument of f be lower-bounded by a sufficiently small positive constant $\tau > 0$, i.e., f is only evaluated for inputs in $[\tau, \infty)$. Then f is thrice differentiable continuously on $[\tau, \infty)$, and all derivatives up to order three are bounded.*

Proof. Let the argument of function f be x ($x > 0$), the first three derivatives of $f(x) = \log(x)$ are

$$f'(x) = \frac{1}{x}, \quad f''(x) = -\frac{1}{x^2}, \quad f^{(3)}(x) = \frac{2}{x^3}.$$

On the restricted domain $[\tau, \infty)$ with $\tau > 0$, each derivative is continuous and satisfies

$$|f'(x)| \leq \frac{1}{\tau}, \quad |f''(x)| \leq \frac{1}{\tau^2}, \quad |f^{(3)}(x)| \leq \frac{2}{\tau^3}.$$

Hence $f \in C^3([\tau, \infty))$ and all derivatives up to order three are uniformly bounded by finite constants. □

Corollary 1 (Convergence of the NMC estimator). *Under the conditions in Lemma 1 and assuming independence between the inner and outer samplers, the mean squared error of $\widehat{U}_{S,J}(\boldsymbol{\xi}_{(b)})$ converges to 0 at rate $O(S^{-1} + J^{-2})$,*

$$\mathbb{E}[(\widehat{U}_{S,J}(\boldsymbol{\xi}_{(b)}) - U(\boldsymbol{\xi}_{(b)}))^2] = O(S^{-1} + J^{-2}).$$

Proof. For notational brevity, let \mathbf{z} denote a generic random variable drawn from the predictive distribution in the MI-based utility function in Equation (11), which can represent either \mathbf{y}^* , $\mathbf{y}_{(b)}^{\text{new}}$, or their joint pair $(\mathbf{y}^*, \mathbf{y}_{(b)}^{\text{new}})$.

Consider the utility function and its NMC estimator,

$$U = \mathbb{E}_{\mathbf{z}}[f(\gamma(\mathbf{z}))], \quad \widehat{U}_{S,J} = \frac{1}{S} \sum_{s=1}^S f(\widehat{\gamma}_J(\mathbf{z}_s)),$$

where the inner Monte Carlo approximation of the predictive marginal density is

$$\gamma(\mathbf{z}) = \int p(\mathbf{z} | \boldsymbol{\Omega}) p(\boldsymbol{\Omega}) d\boldsymbol{\Omega}, \quad \widehat{\gamma}_J(\mathbf{z}) = \frac{1}{J} \sum_{j=1}^J p(\mathbf{z} | \boldsymbol{\Omega}^{(j)}),$$

and the outer-layer function is $f(\cdot) = \log(\cdot)$ as defined in Lemma 1.

Let $\Delta(\mathbf{z}) = \widehat{\gamma}_J(\mathbf{z}) - \gamma(\mathbf{z})$. For fixed \mathbf{z} , the second-order Taylor expansion of f around $\gamma(\mathbf{z})$ gives

$$f(\widehat{\gamma}_J(\mathbf{z})) = f(\gamma(\mathbf{z})) + f'(\gamma(\mathbf{z}))\Delta + \frac{f''(\gamma(\mathbf{z}))}{2}\Delta^2 + \frac{f^{(3)}(\xi)}{6}\Delta^3, \quad \xi \in [\min\{\widehat{\gamma}_J, \gamma\}, \max\{\widehat{\gamma}_J, \gamma\}].$$

By Lemma 1, all derivatives of f up to order three are bounded on $[\tau, \infty)$. Under the standard moment assumptions for the inner Monte Carlo estimator,

$$\mathbb{E}[\Delta | \mathbf{z}] = 0, \quad \mathbb{E}[\Delta^2 | \mathbf{z}] = \frac{\sigma^2(\mathbf{z})}{J}, \quad \mathbb{E}[|\Delta|^3 | \mathbf{z}] \leq \frac{C}{J^{3/2}},$$

for some finite constant $C > 0$ independent of J .

Taking conditional expectations of the Taylor expansion and applying these bounds yields

$$|\mathbb{E}[f(\widehat{\gamma}_J(\mathbf{z})) | \mathbf{z}] - f(\gamma(\mathbf{z}))| \leq \frac{C_1}{J}, \quad \text{Var}(f(\widehat{\gamma}_J(\mathbf{z})) | \mathbf{z}) \leq \frac{C_2}{J},$$

where $C_1, C_2 > 0$ are finite constants depending only on τ^{-1} and bounded moments of $p(\mathbf{z} | \boldsymbol{\Omega})$.

The mean square error (MSE) of the NMC estimator $\widehat{U}_{S,J}$ can be decomposed into three parts: (i) the variance due to the finite outer sample size S ; (ii) the variance due to the inner samples; and (iii) the squared bias introduced by the inner MC approximation:

$$\text{MSE}(\widehat{U}_{S,J}) = \frac{1}{S} \text{Var}_{\mathbf{z}}[f(\gamma(\mathbf{z}))] + \frac{1}{S} \mathbb{E}_{\mathbf{z}}[\text{Var}(f(\widehat{\gamma}_J(\mathbf{z})) | \mathbf{z})] + \mathbb{E}_{\mathbf{z}}\left[\left(\mathbb{E}[f(\widehat{\gamma}_J(\mathbf{z})) | \mathbf{z}] - f(\gamma(\mathbf{z}))\right)^2\right].$$

Substituting the above bounds into, we can obtain

$$\text{MSE}(\widehat{U}_{S,J}) \leq \frac{V_0}{S} + \frac{C_2}{SJ} + \frac{C_1^2}{J^2},$$

where $V_0 = \text{Var}_{\mathbf{z}}[f(\gamma(\mathbf{z}))]$ is also some finite constant. Since U can be regarded as a linear combination of three logarithmic components (one joint and two marginals) and $J \geq 1$, the same rate holds for the NMC estimator $\widehat{U}_{S,J}$:

$$\mathbb{E}\left[(\widehat{U}_{S,J} - U)^2\right] \leq \frac{C'_1}{S} + \frac{C'_2}{J^2},$$

for some finite constants $C'_1, C'_2 > 0$. □

Corollary 2 (Bias and almost sure convergence of the NMC estimator). *For any finite S, J , $\widehat{U}_{S,J}(\boldsymbol{\xi}_{(b)})$ is a biased estimator of $U(\boldsymbol{\xi}_{(b)})$, i.e.,*

$$\mathbb{E}[\widehat{U}_{S,J}(\boldsymbol{\xi}_{(b)})] \neq U(\boldsymbol{\xi}_{(b)}).$$

Under the regularity conditions of Lemma 1, if $J \rightarrow \infty$ and $S \rightarrow \infty$, then $\widehat{U}_{S,J}(\boldsymbol{\xi}_{(b)})$ converges to $U(\boldsymbol{\xi}_{(b)})$ almost surely:

$$\widehat{U}_{S,J}(\boldsymbol{\xi}_{(b)}) \xrightarrow{\text{a.s.}} U(\boldsymbol{\xi}_{(b)}).$$

Proof. (i) (*Bias*). Recall that for each outer sample \mathbf{z}_s , the inner Monte Carlo estimate is

$$\widehat{\gamma}_J(\mathbf{z}_s) = \frac{1}{J} \sum_{j=1}^J p(\mathbf{z}_s | \boldsymbol{\Omega}^{(j)}), \quad \gamma(\mathbf{z}_s) = \mathbb{E}_{\boldsymbol{\Omega}|\mathcal{D}}[p(\mathbf{z}_s | \boldsymbol{\Omega})].$$

Then, the NMC estimator is

$$\widehat{U}_{S,J} = \frac{1}{S} \sum_{s=1}^S f(\widehat{\gamma}_J(\mathbf{z}_s)), \quad U = \mathbb{E}_{\mathbf{z}}[f(\gamma(\mathbf{z}))].$$

By Jensen's inequality, since $\log(\cdot)$ is strictly concave,

$$\mathbb{E}[f(\widehat{\gamma}_J(\mathbf{z})) | \mathbf{z}] = \mathbb{E}[\log(\widehat{\gamma}_J(\mathbf{z})) | \mathbf{z}] \leq \log(\mathbb{E}[\widehat{\gamma}_J(\mathbf{z}) | \mathbf{z}]) = \log(\gamma(\mathbf{z})) = f(\gamma(\mathbf{z})).$$

Hence, $\mathbb{E}[f(\widehat{\gamma}_J(\mathbf{z}))] \leq f(\gamma(\mathbf{z}))$ and the equality only holds if $\widehat{\gamma}_J(\mathbf{z})$ is deterministic (which only happens as $J \rightarrow \infty$). Therefore,

$$\mathbb{E}[\widehat{U}_{S,J}] = \mathbb{E}_{\mathbf{z}}[\mathbb{E}[f(\widehat{\gamma}_J(\mathbf{z})) | \mathbf{z}]] < \mathbb{E}_{\mathbf{z}}[f(\gamma(\mathbf{z}))] = U,$$

showing that the NMC estimator of U is negatively biased for any finite J .

(ii) (*Almost sure convergence*). Because of the strong law of large numbers, the inner Monte Carlo estimator satisfies

$$\widehat{\gamma}_J(\mathbf{z}) = \frac{1}{J} \sum_{j=1}^J p(\mathbf{z} | \boldsymbol{\Omega}^{(j)}, \mathcal{D}) \xrightarrow{\text{a.s.}} \mathbb{E}_{\boldsymbol{\Omega}|\mathcal{D}}[p(\mathbf{z} | \boldsymbol{\Omega}, \mathcal{D})] = \gamma(\mathbf{z})$$

when $J \rightarrow \infty$.

Since $f(\cdot) = \log(\cdot)$ is continuous on $[\tau, \infty)$, the continuous mapping theorem then gives

$$f(\widehat{\gamma}_J(\mathbf{z})) \xrightarrow{\text{a.s.}} f(\gamma(\mathbf{z})).$$

For the outer layer,

$$\widehat{U}_{S,J} = \frac{1}{S} \sum_{s=1}^S f(\widehat{\gamma}_J(\mathbf{z}_s)).$$

For each S , as $J \rightarrow \infty$, we have pointwise convergence $f(\widehat{\gamma}_J(\mathbf{z}_s)) \rightarrow f(\gamma(\mathbf{z}_s))$. Then we use the strong law of large numbers again,

$$\frac{1}{S} \sum_{s=1}^S f(\gamma(\mathbf{z}_s)) \xrightarrow{\text{a.s.}} \mathbb{E}_{\mathbf{z}}[f(\gamma(\mathbf{z}))] = U.$$

Finally we combine the two limits, first $J \rightarrow \infty$, then $S \rightarrow \infty$, and use the dominated convergence theorem to interchange limits if necessary. Thus we obtain the joint almost sure convergence

$$\widehat{U}_{S,J} \xrightarrow{\text{a.s.}} U, \quad \text{as } J \rightarrow \infty, S \rightarrow \infty.$$

This completes the proof. □

Appendix B The computational detail of Algorithm 2

Schur complement block update for $\Sigma_{oo}^{(b)}$. Recall the joint covariance structure at round b in sequential experimental design

$$\text{Cov} \left[\begin{pmatrix} \mathbf{y}^* \\ \mathbf{y}_{(1:b)}^{\text{new}} \\ \mathbf{y} \end{pmatrix} \right] = \begin{pmatrix} \Sigma_{**} & \Sigma_{*(\text{new}, 1:b)} & \Sigma_{*o} \\ \Sigma_{(\text{new}, 1:b)*} & \Sigma_{(\text{new}, 1:b)(\text{new}, 1:b)} & \Sigma_{(\text{new}, 1:b)o} \\ \Sigma_{o*} & \Sigma_{o(\text{new}, 1:b)} & \Sigma_{oo} \end{pmatrix} \in \mathbb{R}^{(n^*+N_o) \times (n^*+N_o)},$$

with $N_o = n + m + b$. The corresponding observation block can be written as

$$\Sigma_{oo}^{(b)} := \begin{pmatrix} \Sigma_{(\text{new}, 1:b)(\text{new}, 1:b)} & \Sigma_{(\text{new}, 1:b)o} \\ \Sigma_{o(\text{new}, 1:b)} & \Sigma_{oo} \end{pmatrix} \in \mathbb{R}^{N_o \times N_o}.$$

Then for the next round $b+1$ we add a new design point $\xi_{(b)}$, and the enlarged observation block matrix can be written in 2×2 form

$$\Sigma_{oo}^{(b+1)} = \begin{pmatrix} \Sigma_{(\text{new}, b+1)(\text{new}, b+1)} & \Sigma_{(\text{new}, b+1)o^{(b)}} \\ \Sigma_{o^{(b)}(\text{new}, b+1)} & \Sigma_{oo}^{(b)} \end{pmatrix}.$$

In this way, all the sub-blocks can be obtained by slicing the precomputed joint covariance over all prediction, candidate design and observation locations. For notational brevity, we introduce

$$\mathbf{A}^{(b)} := \Sigma_{o^{(b)}(\text{new}, b+1)} \in \mathbb{R}^{N_o}, \quad \mathbf{B}^{(b)} := \Sigma_{(\text{new}, b+1)(\text{new}, b+1)} \in \mathbb{R},$$

so that

$$\Sigma_{oo}^{(b+1)} = \begin{pmatrix} \mathbf{B}^{(b)} & \mathbf{A}^{(b)\top} \\ \mathbf{A}^{(b)} & \Sigma_{oo}^{(b)} \end{pmatrix}.$$

Here in this work, although $\mathbf{B}^{(b)}$ is a scalar since only one design point is added at each round, we still keep the boldface notation to maintain a general representation of the block-matrix formulation. If we have computed the inverse of $\Sigma_{oo}^{(b)}$ and cached $(\Sigma_{oo}^{(b)})^{-1}$, the Schur complement (block inverse) update allows us to obtain $(\Sigma_{oo}^{(b+1)})^{-1}$ efficiently. Define

$$\mathbf{u}^{(b)} := (\Sigma_{oo}^{(b)})^{-1} \mathbf{A}^{(b)} \in \mathbb{R}^{N_o}, \quad \lambda^{(b)} := (\mathbf{B}^{(b)} - \mathbf{A}^{(b)\top} \mathbf{u}^{(b)})^{-1} \in \mathbb{R},$$

where $\lambda^{(b)}$ represents the conditional covariance/variance for the newly chosen design inputs. Then we obtain the inverse of $\Sigma_{oo}^{(b+1)}$ by using the Schur complement update

$$(\Sigma_{oo}^{(b+1)})^{-1} = \begin{pmatrix} \lambda^{(b)} & -\lambda^{(b)} \mathbf{u}^{(b)\top} \\ -\lambda^{(b)} \mathbf{u}^{(b)} & (\Sigma_{oo}^{(b)})^{-1} + \lambda^{(b)} \mathbf{u}^{(b)} \mathbf{u}^{(b)\top} \end{pmatrix}.$$

This update only requires a computational cost of $O(N_o^2)$ for each set parameter $\Omega_s^{(j)}$.

Rank-one update for the predictive covariance $\Sigma_{(b)}^*$. After the block inverse $(\Sigma_{oo}^{(b+1)})^{-1}$ is obtained, our final target is to compute the predictive covariance matrix $\Sigma_{(b+1)}^*$.

At round b , the predictive covariance matrix can be expressed as

$$\Sigma_{(b)}^* = \Sigma_{**} - \Sigma_{*o^{(b)}} (\Sigma_{oo}^{(b)})^{-1} \Sigma_{o^{(b)}*}.$$

After adding the new design point $\xi_{(b)}$, the predictive covariance becomes

$$\Sigma_{(b+1)}^* = \Sigma_{**} - \Sigma_{*o^{(b+1)}} (\Sigma_{oo}^{(b+1)})^{-1} \Sigma_{o^{(b+1)}*}. \quad (20)$$

Based on the block inverse derived above, the predictive covariance can be efficiently updated using a rank-one Sherman–Morrison (Sherman and Morrison, 1950) update, rather than recomputing the full inverse by calling GP prediction API at each round b . For notational simplicity, we define

$$\mathbf{v}^{(b)} := \Sigma_{*(\text{new}, b+1)} - \Sigma_{*o^{(b)}} \mathbf{u}^{(b)} \in \mathbb{R}^{n^*},$$

where $\Sigma_{*(\text{new}, b+1)} \in \mathbb{R}^{n^*}$ is the newly prepended column of $\Sigma_{*o^{(b+1)}} = (\Sigma_{*(\text{new}, b+1)}; \Sigma_{*o^{(b)}}) \in \mathbb{R}^{n^* \times (N_o+1)}$. The vector $\mathbf{v}^{(b)}$ is the conditional covariance between the prediction points and the newly chosen points, which can be interpreted as the information brought by the newly chosen design input beyond the existing observation set. Substituting this expression for $(\Sigma_{oo}^{(b+1)})^{-1}$ into the predictive covariance formula in Equation (20) yields the result

$$\Sigma_{(b+1)}^* = \Sigma_{(b)}^* - \lambda^{(b)} \mathbf{v}^{(b)} \mathbf{v}^{(b)\top}.$$

This update requires computing the matrix–vector product $\Sigma_{*o^{(b)}} \mathbf{u}^{(b)}$ and the outer product $\mathbf{v}^{(b)} \mathbf{v}^{(b)\top}$, thus the cost for the rank-one update is

$$O(N_o n^* + n^{*2}) \quad \text{for each } \Omega_s^{(j)}.$$

Total computational complexity Combining the Schur complement update for $(\Sigma_{oo}^{(b+1)})^{-1}$ and the subsequent rank-one update for $\Sigma_{(b+1)}^*$, the computational cost for each candidate design point at each round under $\Omega_s^{(j)}$ is

$$O(N_o^2 + N_o n^* + n^{*2}).$$

References

- Paul D. Arendt, Daniel W. Apley, and Wei Chen. A preposterior analysis to predict identifiability in the experimental calibration of computer models. *IIE Transactions*, 48(1):75–88, 2015. doi: 10.1080/0740817X.2015.1064554.
- M. J. Bayarri, J. O. Berger, R. Paulo, J. Sacks, J. A. Cafeo, J. Cavendish, C. Lin, and J. Tu. A framework for validation of computer models. *Technometrics*, 49(2):138–154, 2007. doi: 10.1198/004017007000000092.
- J. Frédéric Bonnans, J. Charles Gilbert, Claude Lemaréchal, and Claudia A. Sagastizábal. *Numerical Optimization: Theoretical and Practical Aspects*. Universitext. Springer-Verlag, Berlin, 2 edition, 2006. ISBN 3-540-35445-X. doi: 10.1007/978-3-540-35447-5.
- Kathryn Chaloner and Isabella Verdinelli. Bayesian experimental design: A review. *Statistical Science*, 10(3):273–304, 1995. doi: 10.1214/ss/1177009939.
- Thomas M. Cover and Peter E. Hart. Nearest neighbor pattern classification. *IEEE Transactions on Information Theory*, 13(1):21–27, 1967. doi: 10.1109/TIT.1967.1053964.
- Dennis D. Cox, Jeong-Soo Park, and Clifford E. Singer. A statistical method for tuning a computer code to a data base. *Computational Statistics & Data Analysis*, 37(1):77–92, 2001. doi: 10.1016/S0167-9473(00)00057-8.
- Roosbeh Dehghannasiri, Dezhen Xue, Prasanna V. Balachandran, Mohammadmahdi R. Yousefi, Lori A. Dalton, Turab Lookman, and Edward R. Dougherty. Optimal experimental design for materials discovery. *Computational Materials Science*, 129:311–322, 2017. doi: 10.1016/j.commatsci.2016.11.041.
- H. Diao, Y. Wang, and D. Wang. A D-optimal sequential calibration design for computer models. *Mathematics*, 10(9):1375, 2022. doi: 10.3390/math10091375.
- Adam Foster, Martin Jankowiak, Eli Bingham, Paul Horsfall, Yee Whye Teh, Tom Rainforth, and Noah D. Goodman. Variational Bayesian optimal experimental design. In *Advances in Neural Information Processing Systems*, volume 32, pages 14036–14047, 2019. URL <https://papers.nips.cc/paper/9553-variational-bayesian-optimal-experimental-design.pdf>.

- Adam Foster, Martin Jankowiak, Michael O’Meara, Yee Whye Teh, and Tom Rainforth. A unified stochastic gradient approach to designing Bayesian-optimal experiments. In *Proceedings of the International Conference on Artificial Intelligence and Statistics*, volume 108, pages 2959–2969, 2020. URL <http://proceedings.mlr.press/v108/foster20a/foster20a.pdf>.
- Adam Foster, Daniela Ivanova, Ilyas Malik, and Tom Rainforth. Deep adaptive design: Amortizing sequential Bayesian experimental design. In *Proceedings of the International Conference on Machine Learning*, volume 139, pages 3384–3395, 2021. URL <http://proceedings.mlr.press/v139/foster21a/foster21a.pdf>.
- Tilmann Gneiting and Adrian E. Raftery. Strictly proper scoring rules, prediction, and estimation. *Journal of the American Statistical Association*, 102(477):359–378, 2007. doi: 10.1198/016214506000001437.
- Mengyang Gu and Lu Wang. Scaled gaussian stochastic process for computer model calibration and prediction. *SIAM/ASA Journal on Uncertainty Quantification*, 6(4):1555–1583, 2018. doi: 10.1137/17M1159890.
- D. Higdon, M. Kennedy, J. C. Cavendish, J. A. Cafo, and R. D. Ryne. Combining field data and computer simulations for calibration and prediction. *SIAM Journal on Scientific Computing*, 26(2):448–466, 2004. doi: 10.1137/S1064827503426693.
- L. Jeff Hong and Sandeep Juneja. Estimating the mean of a nonlinear function of conditional expectation. In *Proceedings of the 2009 Winter Simulation Conference (WSC)*, pages 1223–1236. IEEE, 2009. doi: 10.1109/WSC.2009.5429428.
- Xun Huan and Youssef M. Marzouk. Simulation-based optimal Bayesian experimental design for nonlinear systems. *Journal of Computational Physics*, 232(1):288–317, 2013. doi: 10.1016/j.jcp.2012.08.013.
- Mark E. Johnson, L. Michael Moore, and Don Ylvisaker. Minimax and maximin distance designs. *Journal of Statistical Planning and Inference*, 26(2):131–148, 1990. doi: 10.1016/0378-3758(90)90122-B.
- Marc C. Kennedy and Anthony O’Hagan. Bayesian calibration of computer models. *Journal of the Royal Statistical Society: Series B (Statistical Methodology)*, 63(3):425–464, 2001. doi: 10.1111/1467-9868.00294.
- Paul D. W. Kirk and Michael P. H. Stumpf. Gaussian process regression bootstrapping: Exploring the effects of uncertainty in time course data. *Bioinformatics*, 25(10):1300–1306, 2009. doi: 10.1093/bioinformatics/btp139.
- Steven Kleinegesse and Michael U. Gutmann. Gradient-based Bayesian experimental design for implicit models using mutual information lower bounds, 2021. URL <https://arxiv.org/abs/2105.04379>.

- Scott Koermer, Justin Loda, Aaron Noble, and Robert B. Gramacy. Augmenting a simulation campaign for hybrid computer model and field data experiments. *Technometrics*, 66(4):638–650, 2024. doi: 10.1080/00401706.2024.2345139.
- Andreas Krause, Ajit Singh, and Carlos Guestrin. Near-optimal sensor placements in gaussian processes: Theory, efficient algorithms and empirical studies. *Journal of Machine Learning Research*, 9:235–284, 2008. doi: 10.1145/1390681.1390689.
- A. Krishna, V. Roshan Joseph, S. Ba, W. A. Brenneman, and W. R. Myers. Robust experimental designs for model calibration. *Journal of Quality Technology*, 54(4):441–452, 2021. doi: 10.1080/00224065.2021.1930618.
- Solomon Kullback and Richard A. Leibler. On information and sufficiency. *The Annals of Mathematical Statistics*, 22(1):79–86, 1951. doi: 10.1214/aoms/1177729694.
- Erin R. Leatherman, Angela M. Dean, and Thomas J. Santner. Designing combined physical and computer experiments to maximize prediction accuracy. *Computational Statistics & Data Analysis*, 113:346–362, 2017. doi: 10.1016/j.csda.2016.07.013.
- Chin-Diew Lin and Bor-Chen Tang. Latin hypercubes and space-filling designs. In Angela Dean, Max Morris, John Stufken, and Derek Bingham, editors, *Handbook of Design and Analysis of Experiments*, pages 613–646. Chapman & Hall/CRC, 2015. doi: 10.1201/b18619-27.
- D. V. Lindley. *Bayesian Statistics: A Review*. CBMS-NSF Regional Conference Series in Applied Mathematics. Society for Industrial and Applied Mathematics (SIAM), 1972. ISBN 0-89871-002-2. doi: 10.1137/1.9781611970654.
- S. Lloyd. Least squares quantization in PCM. *IEEE Transactions on Information Theory*, 28(2):129–137, 1982. doi: 10.1109/TIT.1982.1056489.
- Sébastien Marmin and Maurizio Filippone. Deep gaussian processes for calibration of computer models. *Bayesian Analysis*, 17(4):1341–1371, 2022. doi: 10.1214/21-BA1293.
- Werner G. Müller and Benedikt M. Pötscher. Batch sequential design for a nonlinear estimation problem. In Valerii V. Fedorov, Werner G. Müller, and Ivan N. Vuchkov, editors, *Model-Oriented Data-Analysis II*, pages 77–87. Physica-Verlag, Heidelberg, 1992.
- George L. Nemhauser, Laurence A. Wolsey, and Marshall L. Fisher. An analysis of approximations for maximizing submodular set functions i. *Mathematical Programming*, 14: 265–294, 1978. doi: 10.1007/BF01588971.
- Adam Paszke, Sam Gross, Francisco Massa, Adam Lerer, James Bradbury, Gregory Chanan, Trevor Killeen, Zeming Lin, Natalia Gimelshein, Luca Antiga, et al. Pytorch: An imperative style, high-performance deep learning library. In *Advances in Neural Information Processing Systems*, volume 32 of *NeurIPS*, 2019.

- Benjamin Poole, Sherjil Ozair, Aaron van den Oord, Alexander A. Alemi, and George Tucker. On variational bounds of mutual information. In *Proceedings of the 36th International Conference on Machine Learning*, pages 5171–5180, 2019. URL <http://proceedings.mlr.press/v97/poole19a/poole19a.pdf>.
- Matthew T. Pratola, Stephan R. Sain, Derek Bingham, Michael Wiltberger, and E. Joshua Rigler. Fast sequential computer model calibration of large nonstationary spatial-temporal processes. *Technometrics*, 55(2):232–242, 2013. doi: 10.1080/00401706.2013.775897.
- Luc Pronzato and Werner G. Müller. Design of computer experiments: Space filling and beyond. *Statistics and Computing*, 22:681–701, 2012. doi: 10.1007/s11222-011-9242-3.
- Tom Rainforth, Rob Cornish, Hongseok Yang, Andrew Warrington, and Frank Wood. On nesting monte carlo estimators. In *Proceedings of the 35th International Conference on Machine Learning*, volume 80 of *Proceedings of Machine Learning Research*, pages 4267–4276. PMLR, 2018. URL <https://proceedings.mlr.press/v80/rainforth18a.html>.
- P. Ranjan, W. Lu, D. Bingham, S. Reese, B. J. Williams, C. Chou, F. Doss, M. Grosskopf, and J. P. Holloway. Follow-up experimental designs for computer models and physical processes. *Journal of Statistical Theory and Practice*, 5(1):119–136, 2011. doi: 10.1080/15598608.2011.10412055.
- Carl Edward Rasmussen and Christopher K. I. Williams. *Gaussian Processes for Machine Learning*. MIT Press, Cambridge, MA, 2006.
- A. R. Runnalls. Kullback–leibler approach to gaussian mixture reduction. *IEEE Transactions on Aerospace and Electronic Systems*, 43(3):989–999, 2007. doi: 10.1109/TAES.2007.4383588.
- Elizabeth G. Ryan, Christopher C. Drovandi, James M. McGree, and Anthony N. Pettitt. A review of modern computational algorithms for Bayesian optimal design. *International Statistical Review*, 84(1):128–154, 2016. doi: 10.1111/insr.12107.
- Jerome Sacks, William J. Welch, Toby J. Mitchell, and Henry P. Wynn. Design and analysis of computer experiments. *Statistical Science*, 4(4):409–423, 1989. doi: 10.2307/2245858.
- D. Schieferdecker and Marco F. Huber. Gaussian mixture reduction via clustering. In *Proceedings of the 12th International Conference on Information Fusion (FUSION 2009)*, pages 1536–1543, Seattle, WA, USA, 2009. IEEE.
- Jack Sherman and Winifred J. Morrison. Adjustment of an inverse matrix corresponding to a change in one element of a given matrix. *The Annals of Mathematical Statistics*, 21(1):124–127, 1950. doi: 10.2307/2236561.
- William J. Studden. Optimal designs for integrated variance in polynomial regression. In Shanti S. Gupta and David S. Moore, editors, *Statistical Decision Theory and Related Topics II*, pages 411–420. Academic Press, New York, 1977. doi: 10.1016/B978-0-12-307560-4.50026-0.

- Ö. Sürer, M. Plumlee, and S. M. Wild. Sequential Bayesian experimental design for calibration of expensive simulation models. *Technometrics*, 66(2):157–171, 2023. doi: 10.1080/00401706.2023.2246157.
- Ines Swameye, Thomas G. Müller, Jens Timmer, Sandra Oehler, and Ursula Klingmüller. Identification of nucleocytoplasmic cycling as a remote sensor in cellular signaling by databased modeling. *Proceedings of the National Academy of Sciences of the United States of America*, 100(3):1028–1033, 2003. doi: 10.1073/pnas.0237333100.
- Yan Wang, Xiaowei Yue, Rui Tuo, Jeffrey Hunt, and Jianjun Shi. Effective model calibration via sensible variable identification and adjustment with application to composite fuselage simulation. *The Annals of Applied Statistics*, 14(3):1759–1776, 2020. doi: 10.1214/20-AOAS1353.
- Brian J. Williams, Jason L. Loepky, Leslie M. Moore, and Mason S. Macklem. Batch sequential design to achieve predictive maturity with calibrated computer models. *Reliability Engineering & System Safety*, 96(9):1208–1219, 2011. doi: 10.1016/j.ress.2010.04.017.
- Feng Xie and Yumi Xu. Bayesian projected calibration of computer models. *Journal of the American Statistical Association*, 116(536):1965–1982, 2020. doi: 10.1080/01621459.2020.1753519.